SYSTEMS, SCIENCE AND SOFTWARE

SSS-R-76-2993

EXPLOSION YIELD VERIFICATION, MULTIPLE EXPLOSION SCENARIOS AND THREE-DIMENSIONAL SEISMIC MODELING RESEARCH.

D. G. Lambert
C. F. Petersen
J. M. Savino

Quarterly Technical Report.
For Period May 1, 1976 - July 31, 1976

Sponsored by:
Advanced Research Projects Agency
ARPA Order No. 2551

This research was supported by the Advanced Research Projects Agency of the Department of Defense and was monitored by AFTAC/VSC Patrick AFB, FL 32925, under Contract No. F08606-75-C-0045.

August 1976

P O BOX 1620, LA JOLLA, CALIFORNIA 92038, TELEPHONE (714) 453-0060

AFTAC Project Authorization No. VELA T/6712/B/ETR

Program Code No. 6F10

Effective Date of Contract: May 1, 1975

Contract No. F08606-75-C-0045

Principal Investigator and Phone No.

Dr. John M. Savino (714) 453-0060, Ext. 455

Project Scientist and Phone No.

Dr. Ralph W. Alewine, III (202)325-8484

UNCLASSIFIED
SECURITY CLASSIFICATION OF THIS PAGE (When Data Entered)

REPORT DOCUMENTATION PAGE		READ INSTRUCTIONS BEFORE COMPLETING FORM
1. REPORT NUMBER	2. GOVT ACCESSION NO.	3. RECIPIENT'S CATALOG NUMBER
4. TITLE (and Subtitle) EXPLOSION YIELD VERIFICATION, MULTIPLE EXPLOSION SCENARIOS AND THREE-DIMENSIONAL SEISMIC MODELING RESEARCH		5. TYPE OF REPORT & PERIOD COVERED Quarterly Technical Report May 1, 1976-July 31, 1976 6. PERFORMING ORG. REPORT NUMBER SSS-R-76-2993
7. AUTHOR(s) D. G. Lambert, C. F. Petersen and J. M. Savino		8. CONTRACT OR GRANT NUMBER(s) Contract No. F08606-75-C-0045
9. PERFORMING ORGANIZATION NAME AND ADDRESS Systems, Science and Software P.O. Box 1620 La Jolla, CA 92038		10. PROGRAM ELEMENT, PROJECT, TASK AREA & WORK UNIT NUMBERS Program Code No. 6F10 ARPA Order No. 2551
11. CONTROLLING OFFICE NAME AND ADDRESS VELA Seismological Center 312 Montgomery Street Alexandria, VA 22314		12. REPORT DATE August 1976 13. NUMBER OF PAGES 52
14. MONITORING AGENCY NAME & ADDRESS(if different from Controlling Office)		15. SECURITY CLASS. (of this report) Unclassified 15a. DECLASSIFICATION/DOWNGRADING SCHEDULE

16. DISTRIBUTION STATEMENT (of this Report)

Approved for Public Release, Distribution Unlimited.

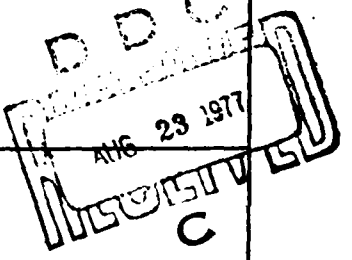

17. DISTRIBUTION STATEMENT (of the abstract entered in Block 20, if different from Report)

18. SUPPLEMENTARY NOTES

19. KEY WORDS (Continue on reverse side if necessary and identify by block number)

Explosion Source Modeling, Yield Determination, Earth Structure, Multiple Explosion Scenarios, Three-Dimensional Seismic Modeling

20. ABSTRACT (Continue on reverse side if necessary and identify by block number)

A procedure for directly inverting teleseismic ground motion data in order to obtain estimates of explosion yields was developed. The particular inversion scheme employs a deterministic modeling capability which predicts the teleseismic ground motion from a nuclear explosion. This procedure supplements expected data exchange packages that provide information on the near explosion source environment.

DD FORM 1 JAN 73 1473 EDITION OF 1 NOV 65 IS OBSOLETE

UNCLASSIFIED
SECURITY CLASSIFICATION OF THIS PAGE (When Data Entered)

Experiments involving computer simulation and decomposition of multiple explosion scenarios were recently initiated. Application of narrow band filtering to synthesized multiple event seismograms has yielded accurate determinations of the relative amplitudes and time separations between individual explosions in the multiple explosion event examined.

Preparations are nearing completion for a series of three-dimensional seismic modeling experiments. The intent of these experiments is to measure differences in signals between single and multiple sources and between near surface and deeply-buried sources. Theoretical explosion calculations will be compared to the experimental results.

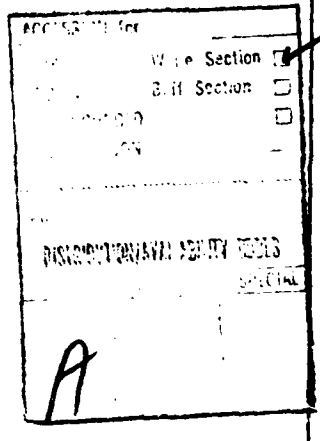

TABLE OF CONTENTS

LIST OF FIGURES

List of Figures (Continued)

I. SUMMARY

During the past several years, Systems, Science and Software (S^3) personnel have been actively engaged in a comprehensive program involving computer modeling of the nonlinear processes that characterize underground nuclear explosions, propagation of the resultant stress wave through realistic earth structures and prediction of the ground motion recorded at teleseismic distances from an explosion. The objectives of the subject project are to employ these modeling and predictive capabilities in a systematic examination of the effects of variations in source and emplacement parameters on seismic signals from underground explosions, and to investigate methods for utilizing the general characteristics of seismic waveforms to obtain reliable yield estimates for explosions.

The technical phases necessary to accomplish the objectives of this project are as follows:

1. Conduct a systematic theoretical examination of material, source and emplacement parameters which affect yield-magnitude relationships and compare the theoretical predictions to actual observations.

2. Determine and express uncertainties of yield estimates in terms of uncertainties in gross earth structure, near source material properties, and local source and receiver structure.

Major accomplishments during the fifth three-month period of this project were realized in several different areas of research. A procedure for directly inverting teleseismic ground motion data in order to obtain explosion yields was developed. The particular inversion scheme is accomplished via a deterministic model which predicts the

teleseismic ground motion for a nuclear explosion. This procedure supplements expected data exchange packages that provide information on the near explosion source environment. Using the data exchange information and inferred interparameter relationships, an equivalent elastic source is computed. Then, estimates of the pP delay time and anelastic properties of the earth's upper mantle, required by the computer ground motion codes, may be obtained from the details of observed teleseismic recordings. The application of this procedure to explosions, reported to be anomalous in terms of accepted magnitude-yield relationships, indicates that interference of the pP and direct P phases (i.e., in the case of the Faultless explosion) and variations in upper mantle attenuation can explain most of the reported anomalies.

Experiments involving computer simulation and decomposition of multiple explosion scenarios were initiated during this report period. The objectives of these experiments are to develop procedures, based on close-in seismic measurements, for verifying the number and yields of individual explosions comprising a multiple event. Close-in seismic data recorded for the underground explosion MAST were used to simulate a simple multiple explosion. This event consisted of a linear array of three equivalent yield explosions, detonated simultaneously.

Application of narrow band filtering to synthesized multiple explosion seismograms yielded accurate relative amplitude and time separation between individual explosions in the scenario. Future scenarios will include more complex source and receiver configurations as well as observed seismograms from several other Pahute Mesa explosions of different yields.

Preparations are nearing completion for the first of four main experiments with three-dimensional seismic models.

The experimental results will be compared with theoretical calculations of the four model experiments. The major tasks presently underway include selection of material, source, detectors and experimental geometry.

II. INTRODUCTION

As stated in the previous section, the objectives of the subject research project are to utilize existing computational capabilities to examine the effects of various source and emplacement parameters on seismic signals from underground explosions, and to devise and evaluate methods for utilizing the general characteristics of seismic waveforms to obtain reliable estimates of explosion yields. In order to realize these objectives, activity on this program during the fifth three-month period of this contract concentrated in the following areas:

1. Inversion of teleseismic ground motion data to obtain explosion yields.
2. The simulation and decomposition of multiple explosion scenarios.
3. Three-dimensional seismic modeling experiments.

The following section of this report is devoted to technical discussions and summaries of each of these three research areas.

III. TECHNICAL DISCUSSION

3.1 TELESEISMIC VERIFICATION OF DATA EXCHANGE YIELDS

A special topical report [Bache, et al., 1976], which addresses the possibility of directly inverting teleseismic ground motion in order to obtain estimates of explosion yields, was written during the last reporting period under this contract. Rather than duplicate the contents of this recent report, we will briefly summarize the important points and conclusions contained therein.

The procedure proposed for accomplishing the inversion of teleseismic data for explosion yield is to employ a deterministic model which predicts ground motion from a nuclear explosion. This procedure makes use of the information expected from the data exchange packages that provide information on the near explosion source environment. Additional parameters that must be inferred from other sources or determined by experiment on geophysical analogues. Key parameters that must be input to the model are the following:

1. The material properties and constitutive behavior of the near source rock environment.
2. The pP-P delay times.
3. The anelastic properties of the earth's upper mantle.

If we can determine the equivalent elastic source for the explosion, then the pP delay time and the anelastic properties of the earth's upper mantle required as input to the deterministic model may be inferred from the details of the recorded ground motion. The report by Bache, et al. [1976] addresses three major categories: equivalent elastic source calculations for a wide range of rock types; the teleseismic amplitude dependence on the source, including the effects of the free surface reflected phase, pP; and the effect of upper mantle elastic properties on short period P waves.

Seven source calculations, corresponding to an explosive device yield of 150 kt at a depth-of-burial of approximately 560 m, were carried out. The rock types considered range from NTS granite (saturated) to shale and sandstone (dry). Of particular significance is the observation of a factor of ten difference in the amplitude of the far-field displacement spectra at 1 Hz between the maximum (weak, saturated tuff) and minimum (strong, dry sandstone) source functions.

The next point addressed is how the source spectra translate into short period seismogram amplitudes at teleseismic ranges; that is, into m_b estimates. Given the equivalent elastic source, it is shown that the teleseismic ground motion is directly proportional to the near source compressional wave speed, α. For purposes of yield verification procedures, this result points up the requirement for in situ measurements of α to be included in a data exchange package. The observed value of α must then be suitably averaged around the source, particularly in the emergent cone for teleseismic rays.

The final section of the report by Bache, et al. [1976] examines the extent to which the amplitude and waveform of teleseismic ground motion is affected by reasonable changes in the structure of the earth's upper mantle. Attention was restricted in this study to the distance range from 20 to 36°. It is shown that reasonable perturbations in the elastic properties of several published upper mantle models [Helmberger and Wiggins, 1971; Wiggins and Helmberger, 1973], produce changes in P wave amplitudes that are less than a factor of two for stations beyond the upper mantle triplications. Within the triplication range (approximately 2000 to 3000 km for most published upper mantle models), variations can be considerably larger.

3.2 SIMULATION AND DECOMPOSITION OF MULTIPLE EXPLOSIONS

3.2.1 Introduction

Recently, we began experimenting with computer simulation and decomposition of multiple explosion scenarios. The objectives of this experiment are to develop procedures, based on close-in seismic measurements, for verifying the number and yields of individual explosions comprising a multiple event. We are also interested in detecting explosions that are detonated concurrently with a multiple event but are located outside the array. Particular tasks to be addressed in the course of this experiment are the following:

- Determine the optimum number and configuration of recording stations required.
- For a given sensor bandpass and background noise characteristics, determine the optimum signal bandpass.
- Examine the sensitivity of the detecting system to the relative spacing, yields, delay times and number of explosions comprising a multiple event.

In the following subsections of this report we describe preliminary results for a simple multiple event. This event was simulated using close-in seismograms recorded by Sandia Laboratories for the Pahute Mesa explosion, MAST. Future experiments will include more complex source and receiver configurations as well as observed seismograms from several other Pahute Mesa explosions of different yields (e.g., Almendro, Colby and Pool).

3.2.2 Experiment Design and Data

The data selected for the first multiple event scenario consisted of close-in seismic measurements of the single,

contained, underground explosion MAST detonated June 19, 1975, in the Pahute Mesa region at NTS. These data were obtained in digital format from Sandia Laboratories in Albuquerque, New Mexico, and include accelerometer and velocity gauge seismograms recorded in the distance range from ground zero to about 8 kilometers from MAST. The digital data were sampled at a rate of 500 points per second.

The explosion and recording station configuration used for the simulated multiple event are shown in Figure 3.1. The test scenario consisted of a linear array of three equivalent yield explosions, equally spaced (355 m) and detonated simultaneously. The explosion spacing of 355 m was taken as representative of row cratering shots in the yield range near 150 kt.

In the numerical simulations to be discussed herein, actual vertical component velocity recordings of the MAST explosion were used. The simulated composite velocity seismograms were constructed at each of the stations along the in-line and 45° profiles shown in Figure 3.1 by delaying and summing the actual MAST seismograms recorded at the (approximate) corresponding distances. The delays were based on the spacings between shots, the propagation velocity assumed and the azimuth to the recording station.

An example of the construction of a seismogram for the multiple event is given in Figure 3.2. This seismogram is for Station 3 along the in-line profile. The delay times were computed assuming a crustal propagation velocity of 3.8 km/sec; this value is equal to the average overburden velocity in the vicinity of the MAST explosion according to measurements reported in the Containment Evaluation Panel (CEP) report prepared for this event.

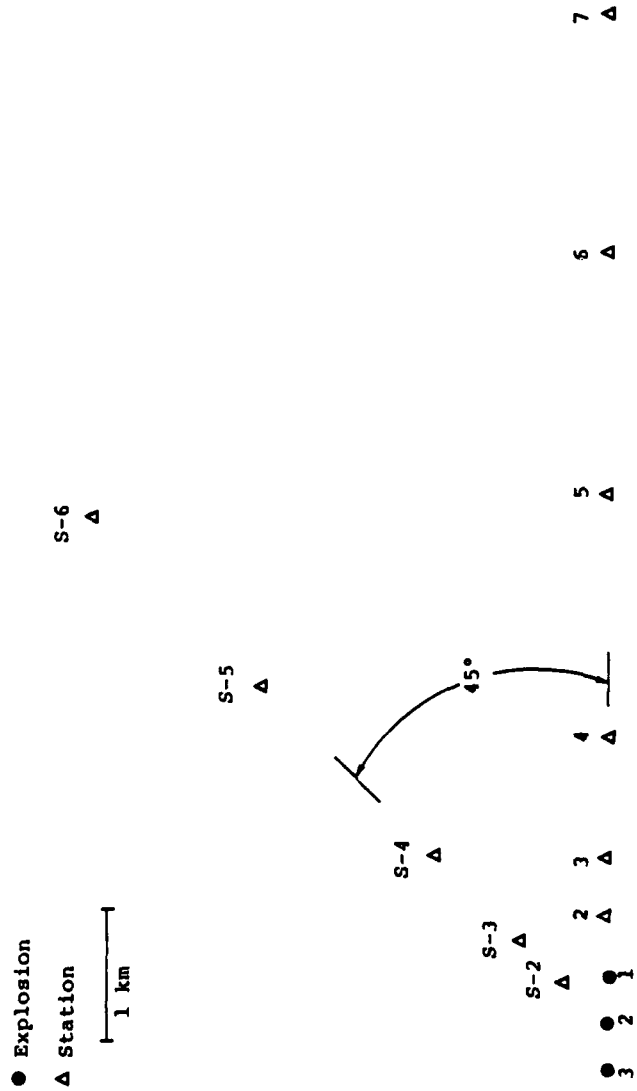

Figure 3.1. Explosion and station configuration.

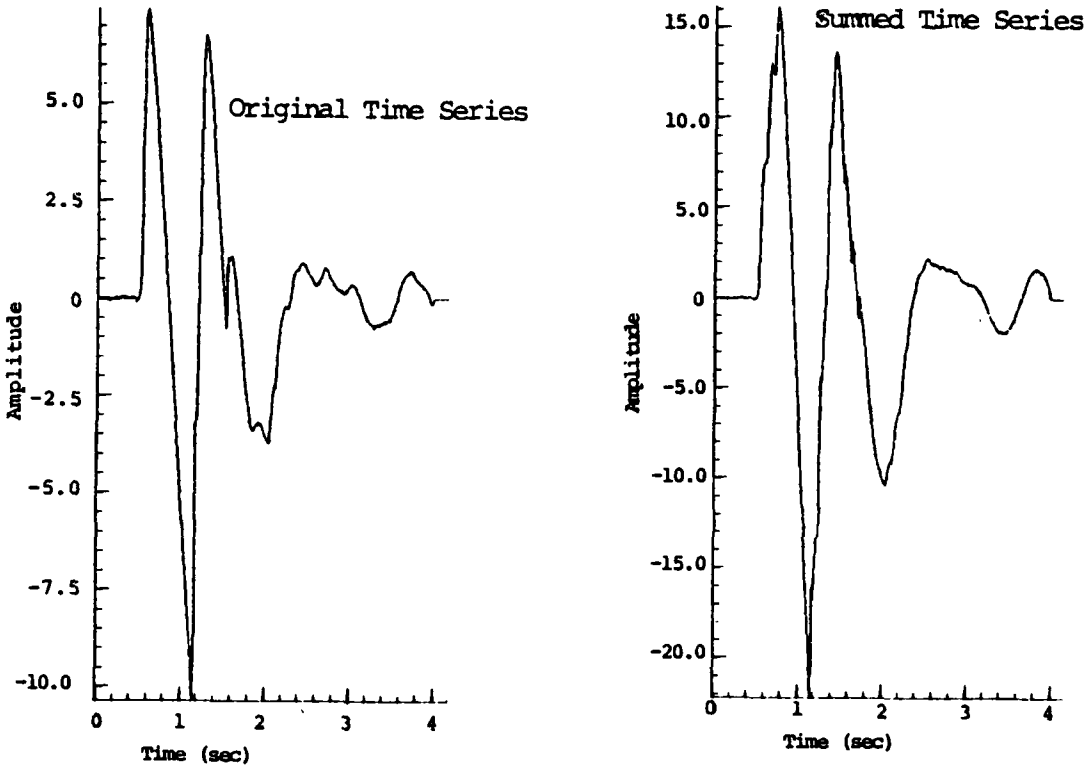

Figure 3.2. Original MAST signal at Station 3 and composite signal along the profile in-line with the shot array.

On the left-hand side of Figure 3.2 we show the actual vertical component velocity seismogram recorded at Station 3 for MAST. The distance range in this case is 0.912 km. The multiple explosion time series is shown on the right-hand side of Figure 3.2. Comparing the original and composite signals we see that, except for the change in peak-to-peak signal amplitude, the superposition of the delayed signals from the three explosions results in only subtle changes in the shape of the waveform. It is quite likely that an analyst would not interpret this seismogram as that from a multiple explosion. In the following sections of this report we will describe the methods used for decomposing this and similar multiple time series.

3.2.3 Signal Analysis Procedure

Decomposition of a complex time series (e.g., Figure 3.2) can be accomplished with the use of a series of narrow-band filters. These filters separate the time series into a set of quasi-harmonic modulated "signals". This procedure was adopted in the MARS signal analysis program employed in this experiment and, as will be shown in the following, can be used to separate and scale multiple explosion scenarios as long as there is sufficient energy (good signal-to-noise ratio) at frequencies near T^{-1} Hz. Here, T is the delay time between primary arrivals recorded at a particular sensor from individual explosions comprising a multiple event.

Figures 3.3 and 3.4 are two different versions of the flow of operations in the MARS signal analysis program. Figure 3.3 gives a verbal outline while Figure 3.4 summarizes the key mathematical operations performed in this program. More detailed descriptions of the theory and operation were presented in Bache, et al. [1975] and Savino, et al. [1975].

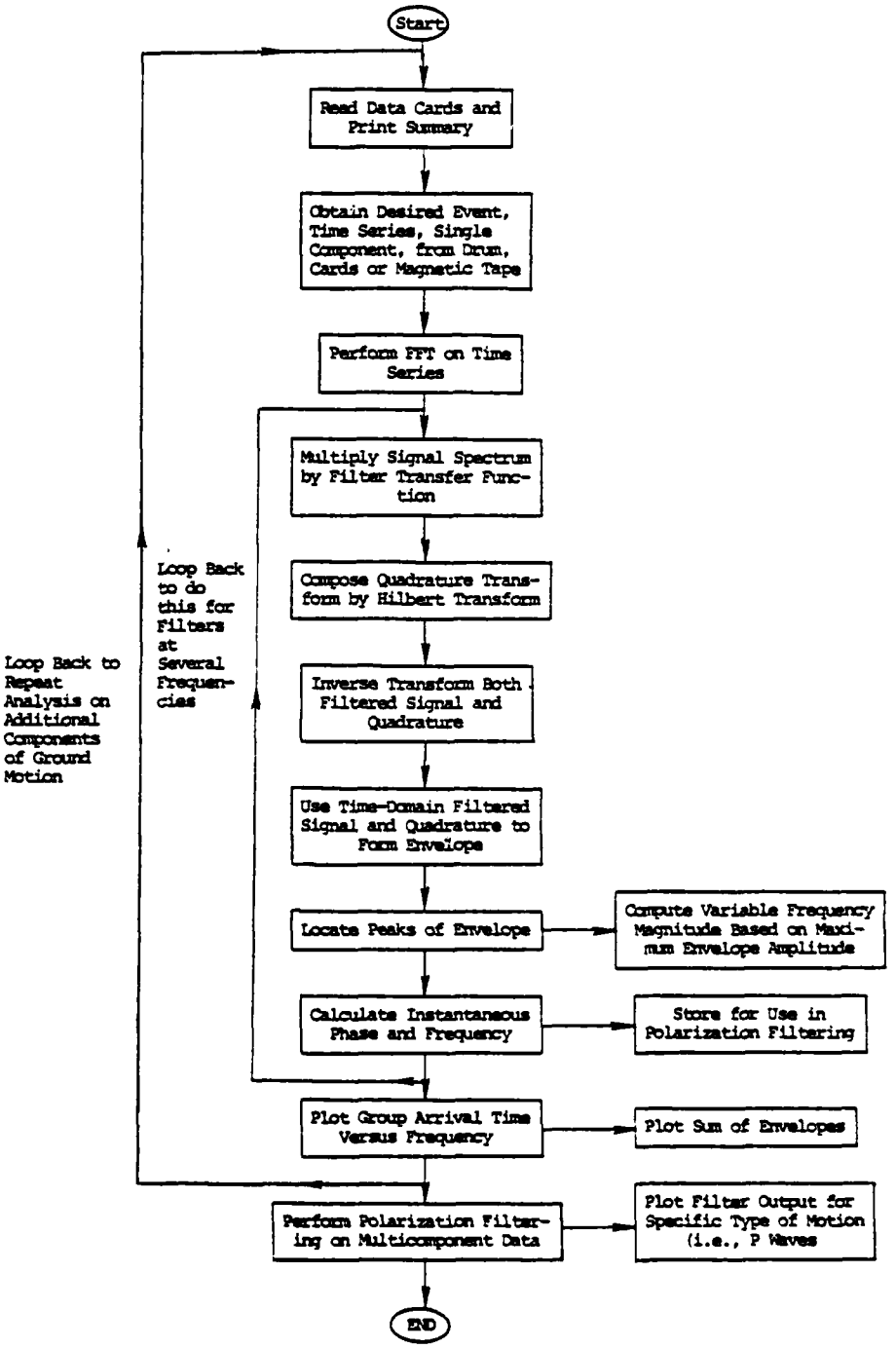

Figure 3.3. MARS flowchart.

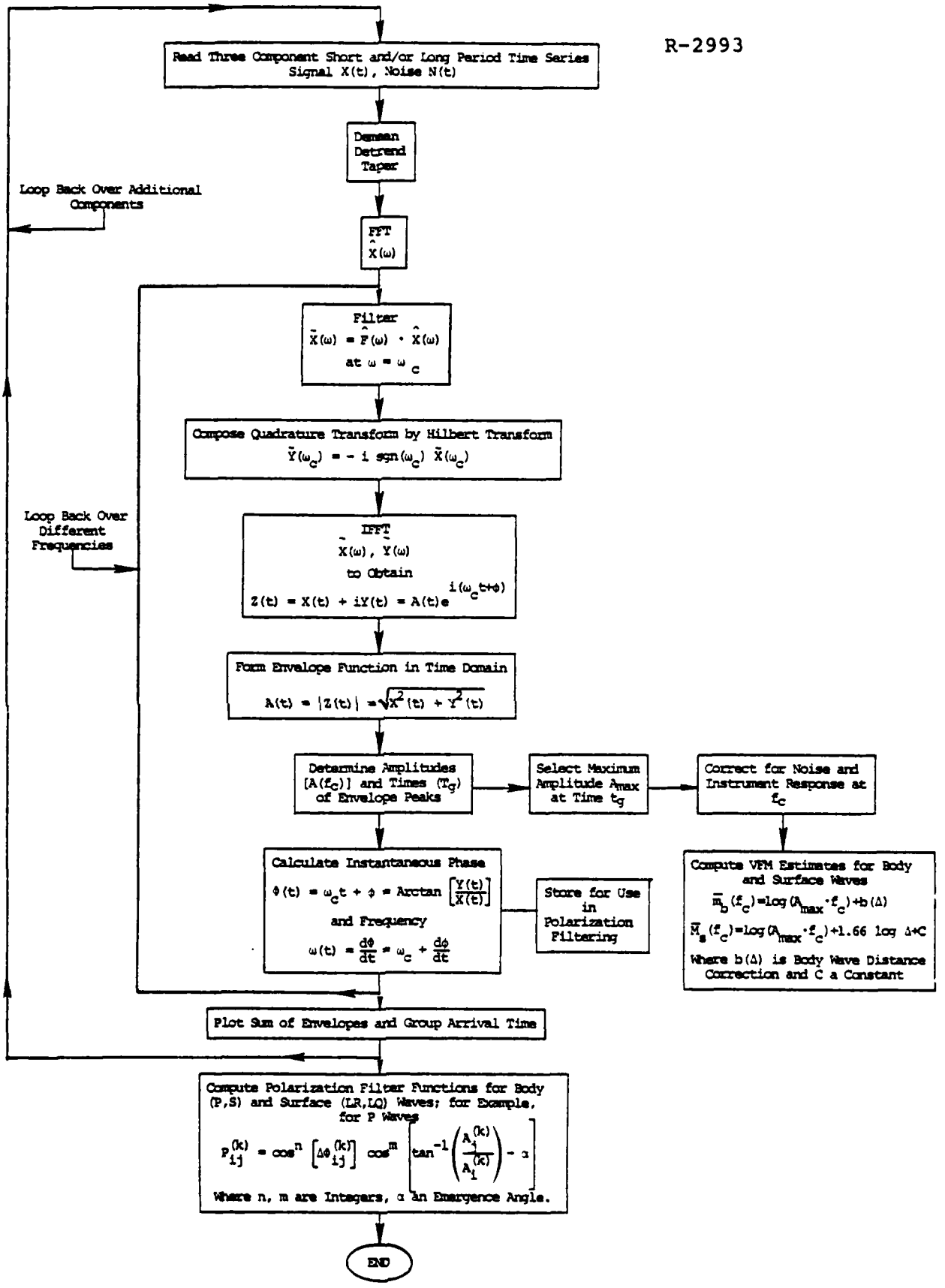

Figure 3.4. Flowchart indicating principal mathematical operations embodied in the MARS program.

Seismic data are read into MARS in the form of a time series (Figures 3.3 and 3.4) generally of about 500-2000 points in length. The data are then optionally detrended, mean removed and tapered at the tail end by a cosine bell. The program then selects the smallest power of two which is greater than the number of points input and performs a discrete Fourier transform using the algorithm of Cooley and Tukey [1965]. Both the original time series and the spectrum are plotted for examination.

Referring to Figures 3.3 and 3.4, the signal is next filtered in the frequency domain by multiplication with a narrow band cusp-shaped filter of the form:

$$F(f) = \begin{cases} 1 - \cos \frac{\pi}{3} \left[\frac{f - \left(f_c - \frac{3}{2} \Delta f \right)}{\Delta f} \right], & f_c - \frac{3}{2} \Delta f \leq f \leq f_c \\ 1 - \cos \frac{\pi}{3} \left[\frac{\left(f_c + \frac{3}{2} \Delta f \right) - f}{\Delta f} \right], & f_c \leq f \leq f_c + \frac{3}{2} \Delta f \\ 0, \text{ otherwise} . \end{cases}$$

This particular filter form, shown in Figure 3.5, was selected to satisfy two goals: (1) minimum width in the frequency domain, and (2) maximum ripple suppression in the time domain. A well-known consequence of the Uncertainty Principle (Sampling Theorem to electrical engineers) is that one cannot simultaneously satisfy these two goals to arbitrary precision. The filter employed was selected for its optimal time and frequency domain characteristics within the limits of the Uncertainty Principle.

Once the signal has been narrow band filtered, it is corrected for the appropriate instrument response; the filtered signal transform is divided by the instrument transfer function. The resulting complex spectrum is then inverse

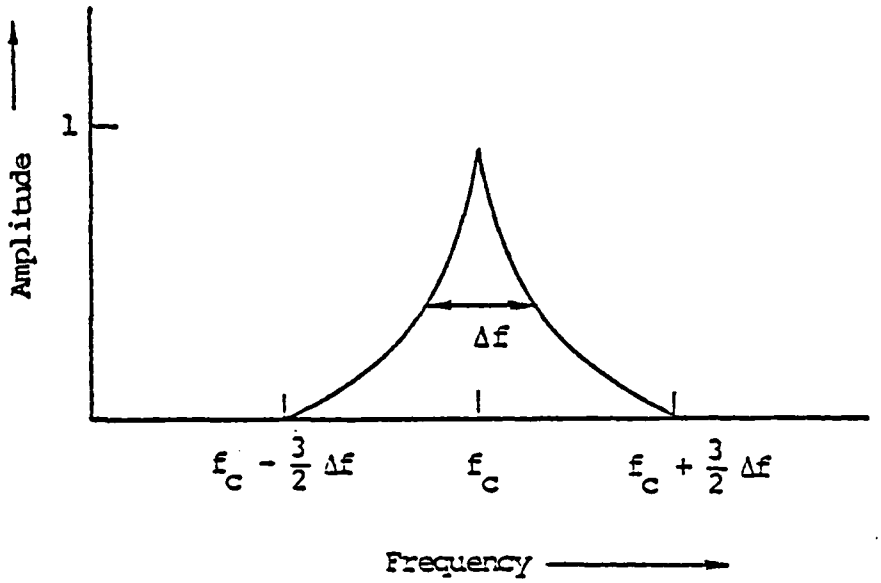

Figure 3.5. Narrow band filter used in MARS. The width at one-half maximum amplitude is designated Δf and for this experiment is set equal to 0.2.

Fourier transformed into the time domain, to produce what will hereafter be referred to as the filtered signal.

The narrow band filtered signal will appear as a quasi-sinusoidal carrier wave contained within a smooth envelope. The next step in the program (Figures 3.3 and 3.4) is to construct the envelope function by means of the Hilbert transform. This method is followed in MARS: the transform of the filtered signal is multiplied by $-i\ \mathrm{sgn}(\omega)$ and then brought to the time domain by an inverse transformation. The maximum of the envelope function is utilized for $m_b(f)$ estimates while the instantaneous frequency and phase are stored for subsequent use in polarization filtering with additional components of ground motion.

The narrow band filtering procedure can be performed on a particular component seismogram (time series) at a number of different frequencies within some band of interest. Correlation of the resulting envelope functions indicates the arrival times of the various frequency components. As an example of the separation of different phase arrivals that can be achieved by the narrow band filtering procedure in MARS, we describe the results of a close-in multiple explosion experiment in the following sections of this report.

3.2.4 Decomposition of Multiple Events

In this portion of the report we first give a rather detailed example of the narrow band filtering operations for a particular multiple event recorded at a selected station to familiarize the reader with the methods employed. The selected station is number 3 on the profile in-line with the shot array. We continue with less detail for the other stations of this profile. This is followed with the important analytical results for the profile of stations oriented 45° to the explosion array.

3.2.4.1 Experimental Results for the Profile of Stations In-Line with the Explosion Array

In Figure 3.2 we showed the original velocity record for Station 3 located 0.912 km from MAST. We also showed the composite or summed velocity record for Station 3 on the profile in-line with the three shots. The delays are based on the spacing between shots (355 m) and a velocity of 3.8 km/sec. Hence, delay times of 0.093 seconds are appropriate (0.355 km/3.8 (km/sec) = 0.093 sec) for all stations along this profile.

A series of 16 narrow band filters with center frequencies (f_c) ranging from 25 to 100 Hz was applied to both the original and composite signal shown in Figure 3.2. The time series output from these filters is shown in Figure 3.6. For the original MAST record at Station 3, three major bursts of high frequency energy occur for this band of frequencies (Figure 3.6a). The times are 0.55, 1.2 and 1.55 seconds. Since we have not attempted to interpret these records, we will not attempt to discuss the origin of these high frequency energy bursts. However, the important fact remains that there is a high signal-to-noise ratio (S/N) at these frequencies. The significance of this result is shown in Figure 3.6b when the same set of filters is applied to the composite (three explosions) event. Here the three major high frequency bursts of energy now show triple peaks where before there was only one. Separation begins at about 40 Hz and becomes increasingly clear with increasing frequency.

Using the Hilbert transform procedure mentioned previously, envelope functions were constructed for each of the sixteen filter outputs. The envelope functions are shown in Figure 3.7a and b for the original and composite signals, respectively. The important point to note (Figure 3.7b) is the clear separation of the three arrivals, corresponding to

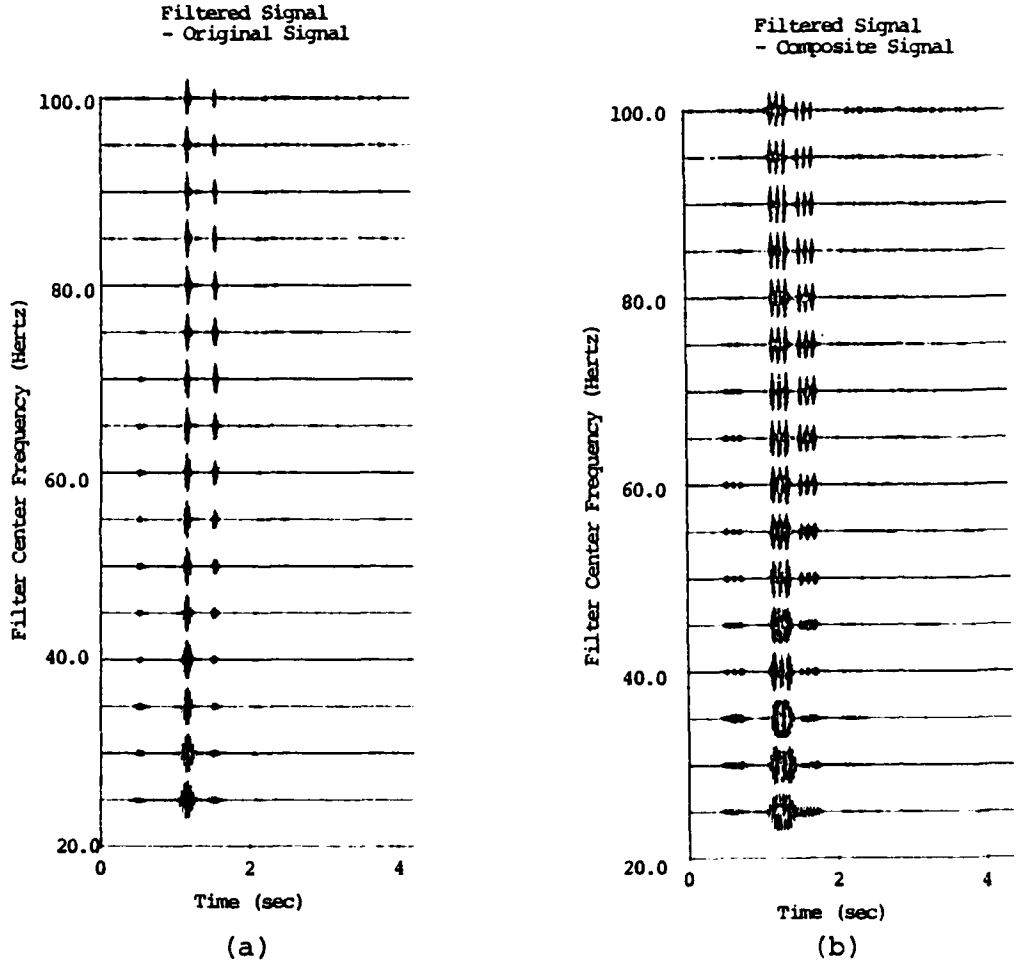

Figure 3.6. Narrow band filtered signals (as functions of frequency and time) for the original (a) and composite (b) signals for Station 3 (Figure 3.2) along the profile in-line with the shot array.

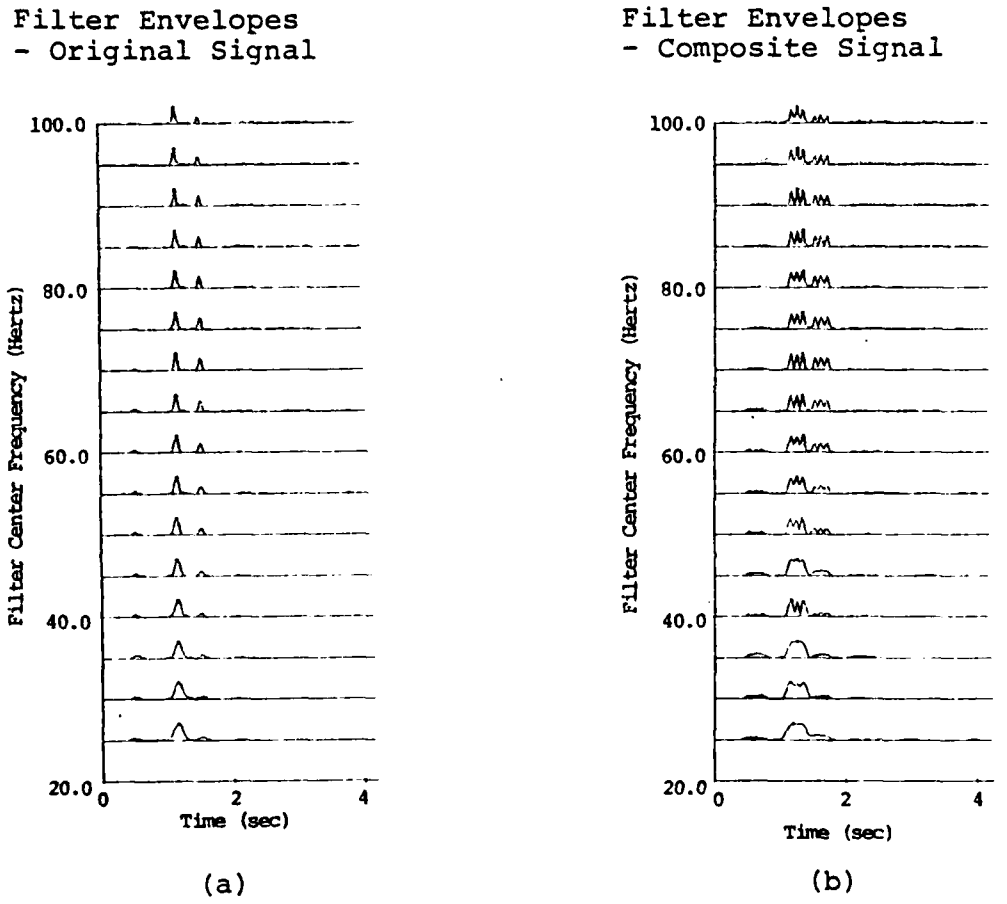

Figure 3.7. Envelope functions (as functions of frequency and time) for narrow band filtered original (a) and composite (b) signals for Station 3 (Figure 3.1) along the profile in-line with the shot array.

the three explosions in the scenario. This separation is even more dramatic in Figure 3.8b, where the sum of the envelopes at the different frequencies (Figure 3.7b) is plotted for the composite signal. A similar sum is plotted for comparison in Figure 3.8a for the original signal.

The time separations of the maximum power arrivals between 1.0 and 1.4 seconds in Figure 3.8b correspond as well as can be determined to the time delays (0.093 seconds) associated with the equal spacings of the three simulated bombs. In addition, note that while the amplitude of the composite signal in Figure 3.2 is more than twice the amplitude of the original signal in Figure 3.2, each peak in the composite envelope sum is nearly equal in amplitude to the peak amplitude of the original unsummed signal.

Similar results are obtained for Stations 2 and 4 in this profile. Figure 3.9 shows the results of the analysis of the composite signal for Station 2. Again, three major high frequency energy levels are observed. Separation due to the three explosions occurs at about 40 Hz and becomes more distinct with increasing frequency (Figure 3.9). Average time separation of the triple peaks is 0.093 and 0.093 seconds, respectively. The observed delay times correspond almost exactly to the input delay times (Table 3.1).

For Stations 5, 6 and 7, high frequency noise dominates the records and the high frequency signal energy, if present, is too low level to obtain any definitive results. Figure 3.10 shows the composite record and analysis for Station 7 and is typical of the three stations.

3.2.4.2 Experimental Results for the Profile of Stations 45° from the Explosion Array

Composite or summed seismograms for the stations oriented at a 45° azimuth from the explosion are shown in Figures 3.11 and 3.12. Delay times were determined relative

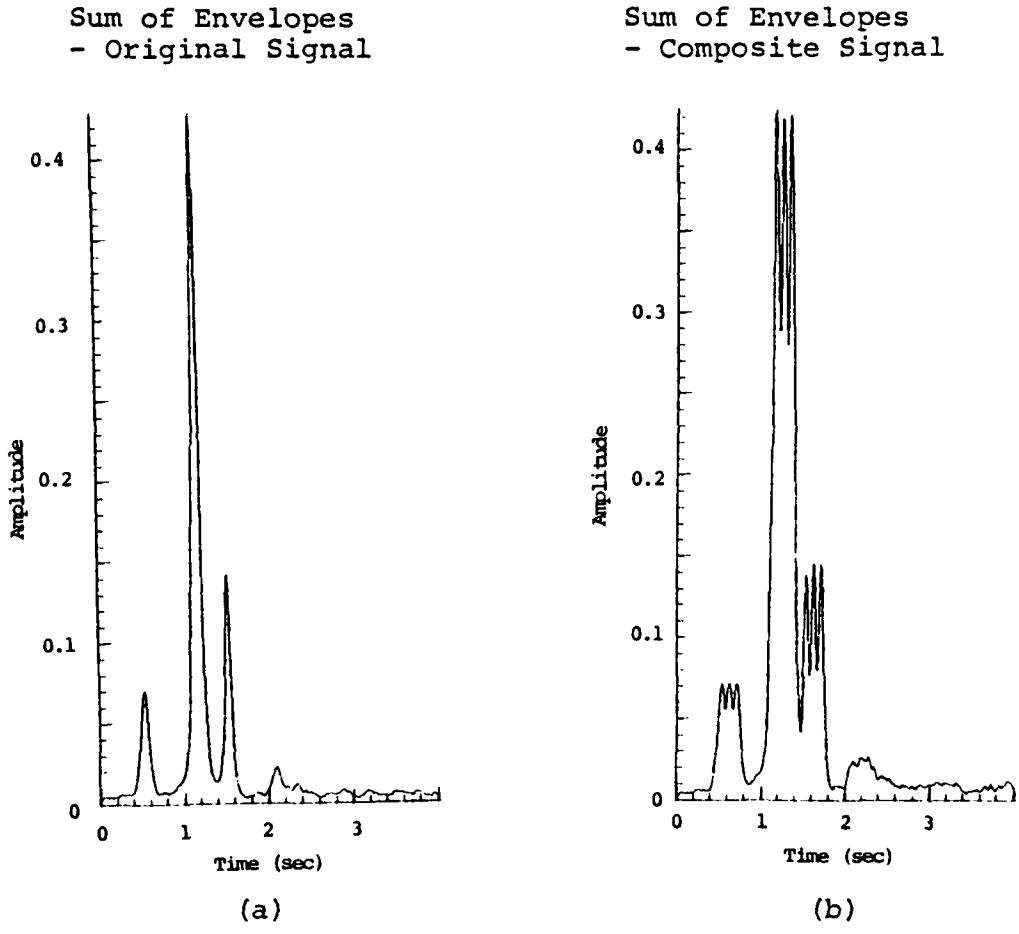

Figure 3.8. Sum of the envelopes shown in Figure 3.7 for the original (a) and composite (b) signals for Station 3 along the profile in-line with the shot array.

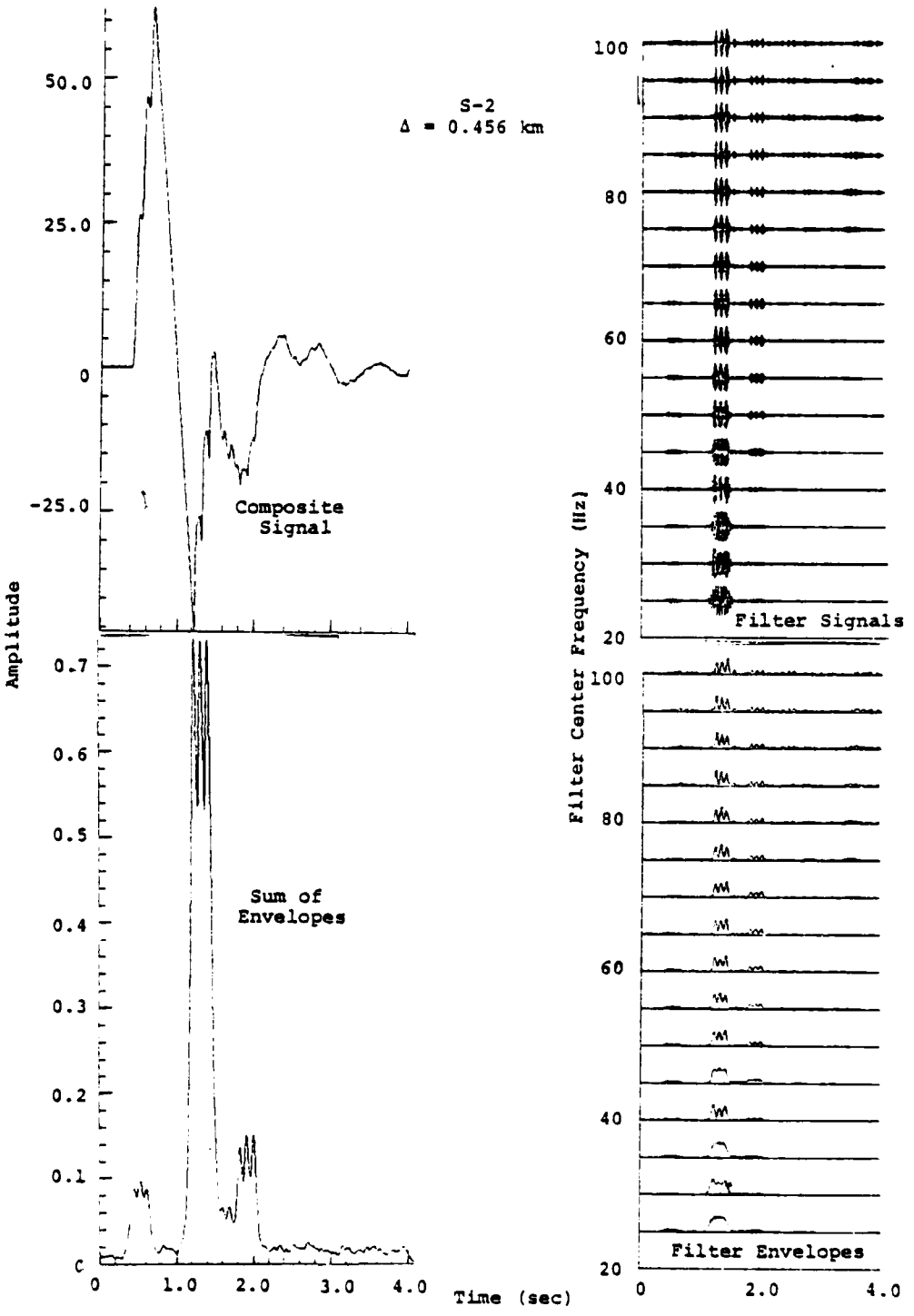

Figure 3.9. Composite signal and sum of envelopes and corresponding filtered signals and filter envelopes at Station 2 for the profile in-line with the shot array.

TABLE 3.1

INPUT DELAY TIMES VERSUS OBSERVED DELAY TIMES

Station \ Shot	Input Delay Times For Stations In-Line With Shot Array (sec)		Observed Delay Times For Stations In-Line With Shot Array (sec)		Input Delay Times For Stations Along 45° Profile Relative to Shot #2 (sec)		Observed Delay Times For Stations Along 45° Profile Relative to Shot #2 (sec)	
2	1-2 0.093	2-3 0.093	1-2 0.091	2-3 0.093	1-2 0.034	2-3 0.076	1-2 0.034	2-3 0.076
3	0.093	0.093	0.093	0.092	0.053	0.072	0.052	0.073
4	0.093	0.093	0.092	0.093	0.061	0.069	0.060	0.070
5	0.093	0.093	--	--	0.062	0.067	--	--
6	0.093	0.093	--	--	0.063	0.066	--	--
7	0.093	0.093	--	--	0.064	0.066	--	--

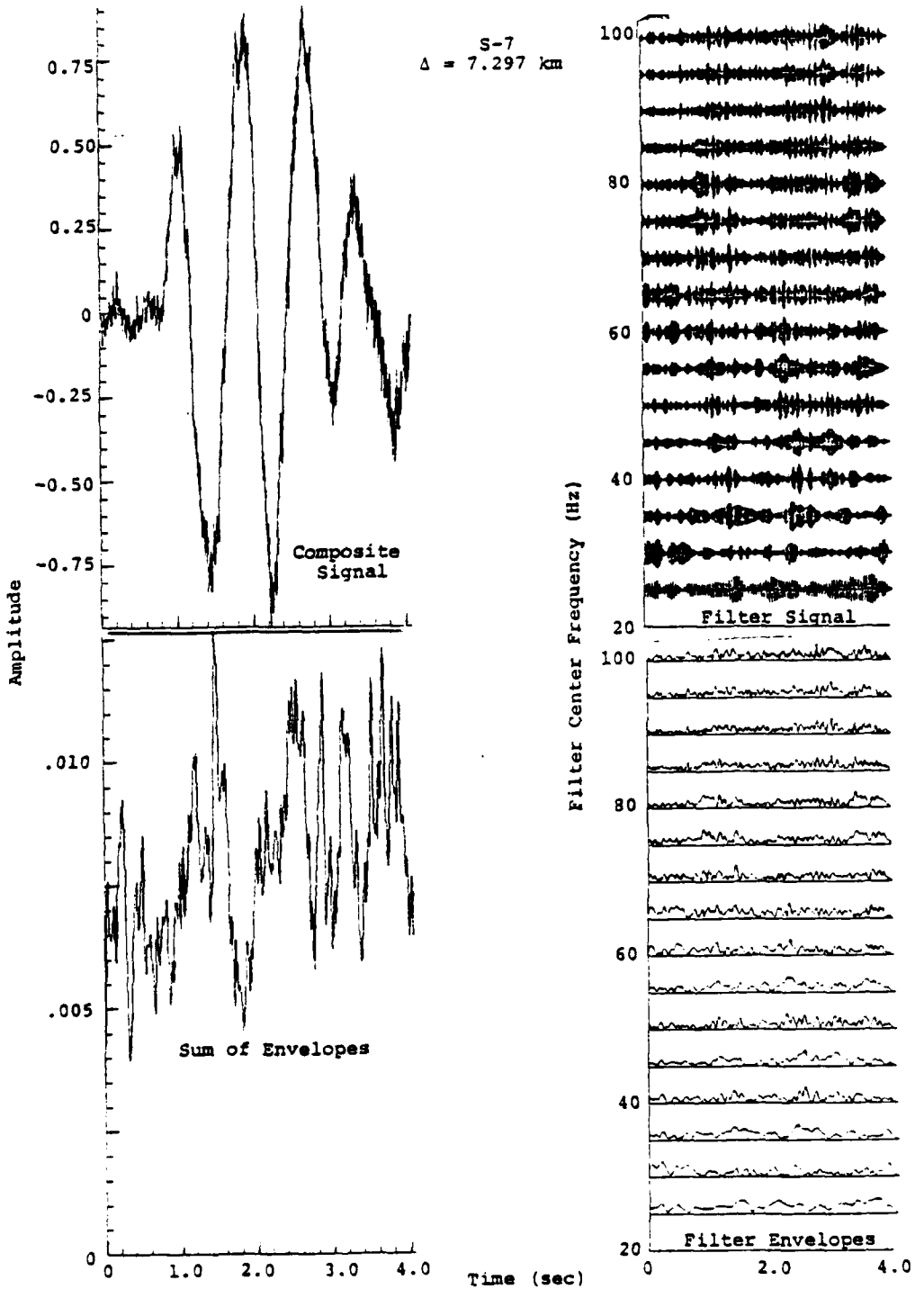

Figure 3.10. Composite signal and sum of envelopes and corresponding filtered signals and filter envelopes at Station 7 for the profile in-line with the shot array.

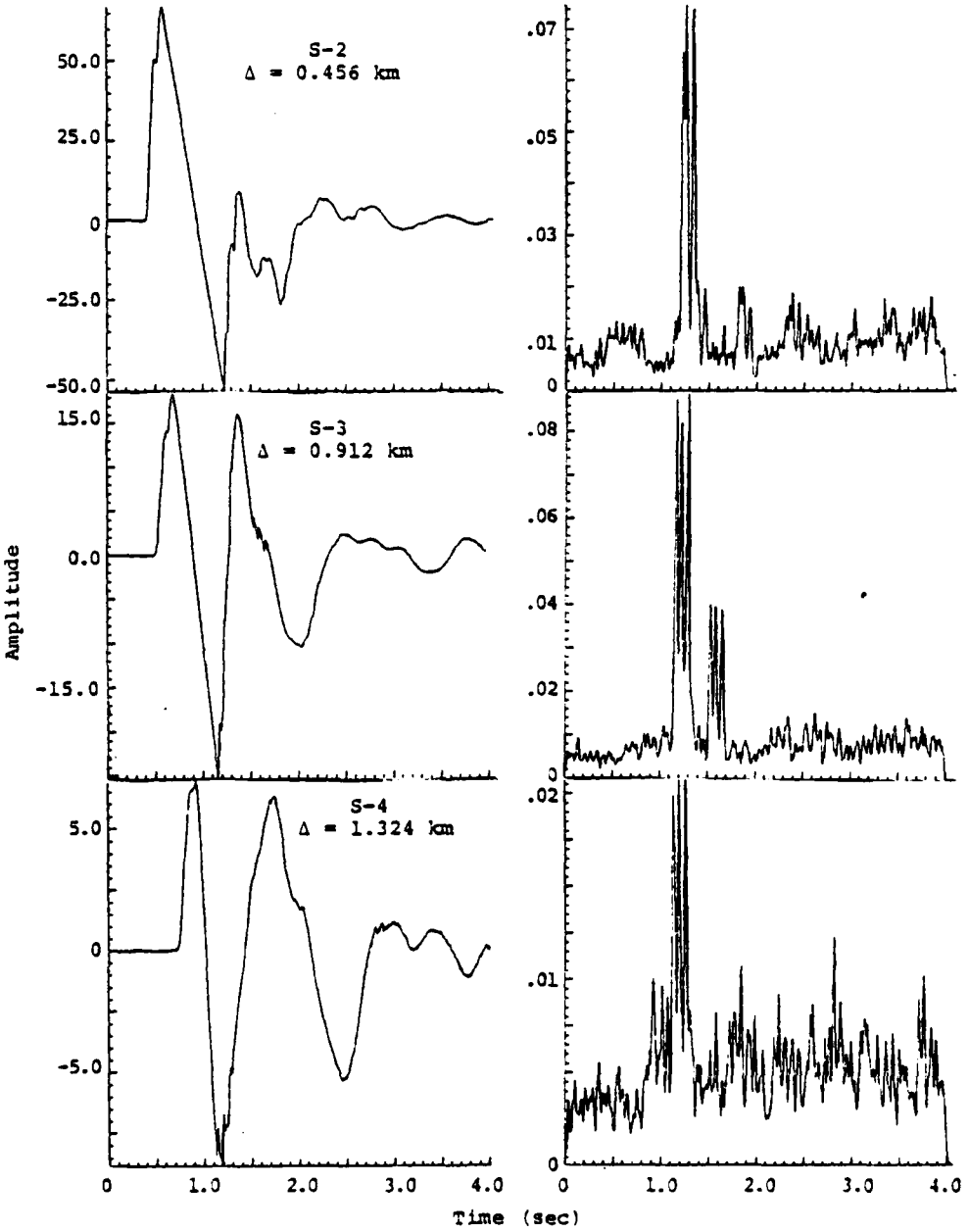

Figure 3.11. Composite signals and corresponding sum of envelopes for Stations S-2, S-3 and S-4 along the 45° profile shown in Figure 3.1.

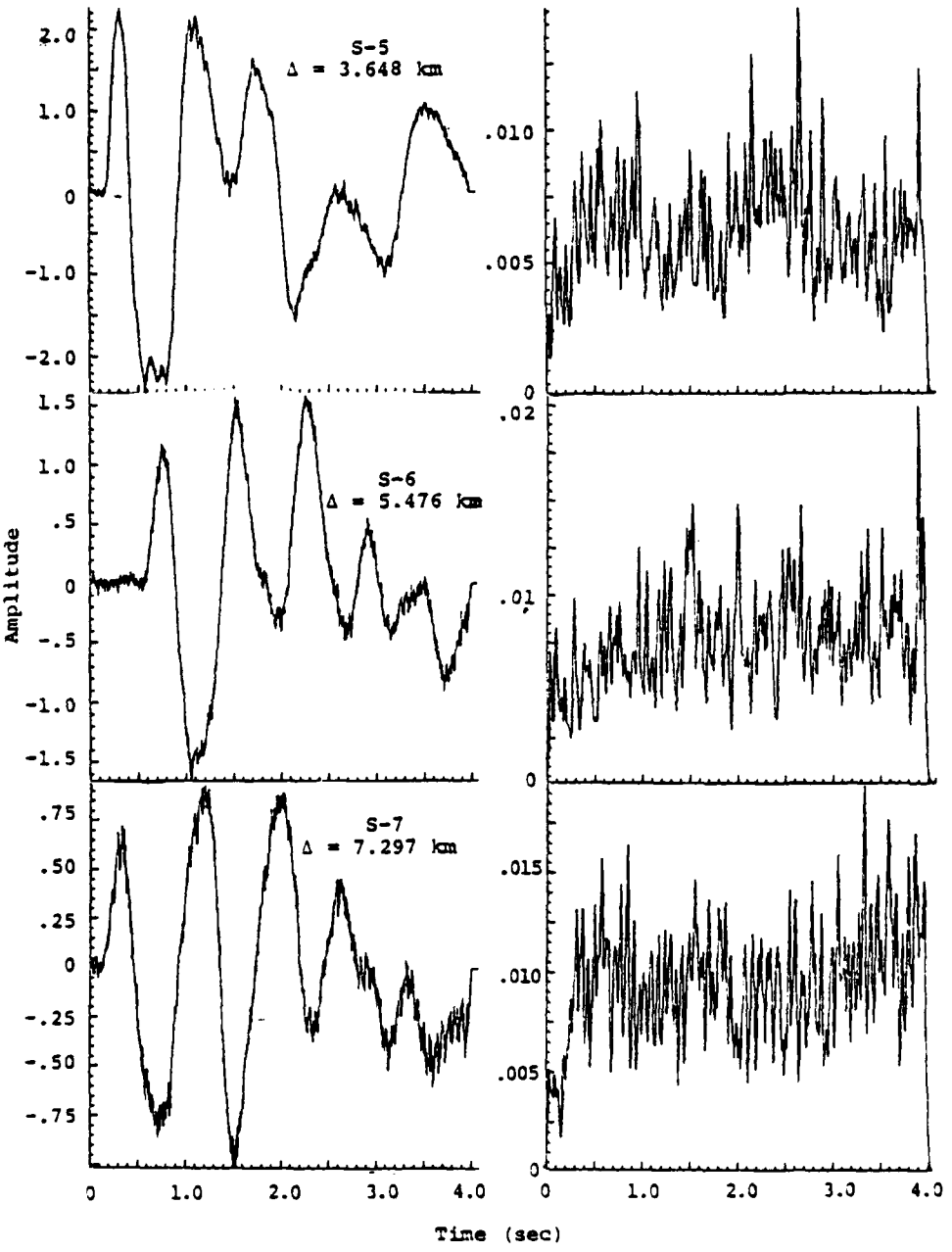

Figure 3.12. Composite signals and corresponding sum of envelopes for Stations S-5, S-6 and S-7 along the 45° profile shown in Figure 3.1.

to the center explosion position (number 2 in Figure 3.1) and are listed in Table 3.1. The delay times vary and are less than those for the in-line array. From the experimental results obtained for the in-line profile of stations, separation (triple peaks) of the explosion energy was observed at about 40 Hz. This frequency is about 3.5 times the diagnostic frequency (inverse of the input explosion delay times of 0.093 seconds) for this station.

Since the delay times for this array of stations are less than those for the previously discussed array, a lower bound for the selection of the range of narrow band filter frequencies (f_c) can be estimated. The smallest delay time of 0.034 seconds occurs at Station S-2 (Table 3.1). This corresponds to a diagnostic frequency of 29.4 Hz. Based on our experience with the previous profile, we would expect separation to occur at about 3.5 times greater than 29.4 Hz or 100 to 105 Hz. Thus, seventeen narrow band filter center frequencies (f_c) ranging from 80 to 160 Hz were selected for analyzing this profile of stations.

In Appendix A we show the narrow band filter outputs for all stations in this profile. For Station S-2 we find that the filter outputs do show that separation for this small increment of time (0.034 sec) begins at 100 Hz.

The results of the narrow band filtering are shown in Figures 3.11 and 3.12 and are summarized in Table 3.1. Stations S-2, S-3 and S-4 do show triple peaks where the signal-to-noise ratio is good at diagnostic frequencies (note the summed envelope functions in Figure 3.11). Further, the amplitudes vary less than 10 percent. Figure 3.12 shows the summed envelope functions for Stations S-5, S-6 and S-7. Here the signal-to-noise ratio is too low in the frequency band of interest (80 to 100 Hz) and no positive results are obtained.

3.2.5 Signal to Noise Comparison

For distances greater than 1.5 kilometers, we obtained no positive results for both station profiles in separating the individual explosions from the explosion array. We stated that this was due to low signal-to-noise ratio in the frequency band of interest (25 Hz to 160 Hz). To show this more clearly, we selected the signal at Station S-7 and a noise sample immediately preceding this signal for analysis (Figure 3.13).

Figure 3.14 shows the corresponding Fourier amplitude spectra. Here the spectral amplitude levels appear about equal for the frequency band of about 30 Hz to 200 Hz. The spectrum for the noise appears to have peaks at 60 Hz and 120 Hz. However, corresponding peaks may or may not be present for the signal spectrum.

In Figure 3.15 we have plotted the peak amplitudes from a series of 19 narrow band filters spanning the frequency range of 25 to 160 Hz, obtained by their application to the described signal and noise samples. It is now clear that both the signal and noise levels are approximately the same. In addition, both samples show strong amplitude peaks at 60 and 120 Hz.

Thus, the signal to noise ratio at Station 7 is essentially zero and 60 Hz noise strongly affects the high frequency portion of the spectrum.

Forming composite records by simple delaying and summation should, in general, increase the high frequency energy content. In Figure 3.15 we have also plotted the peak amplitudes of the composite record for Station 7 along the in-line profile. The peak amplitude level is about two times that of the original signal and noise levels.

Thus, for this analysis the presence of additive high frequency noise, due to the formation of composite records by

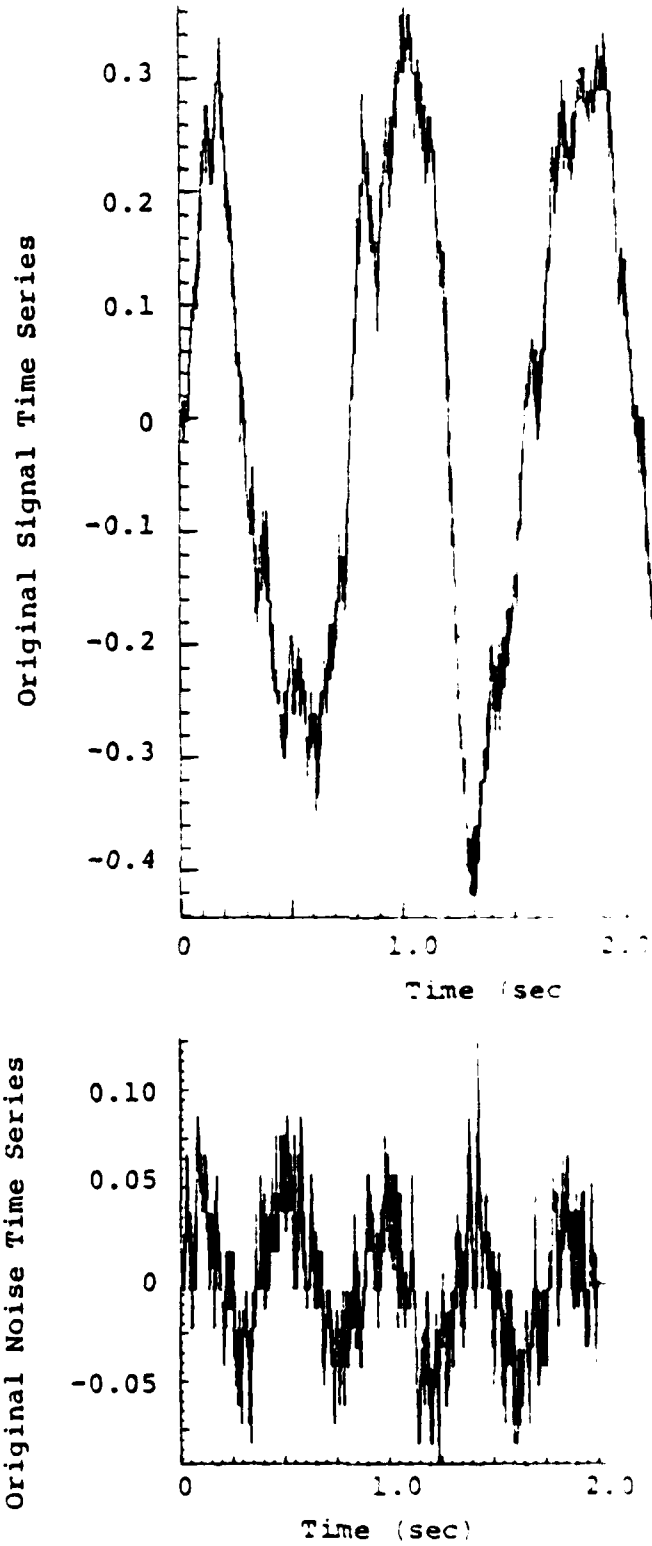

Figure 3.13. Original signal and noise time series from Station 7 of the MAST explosion.

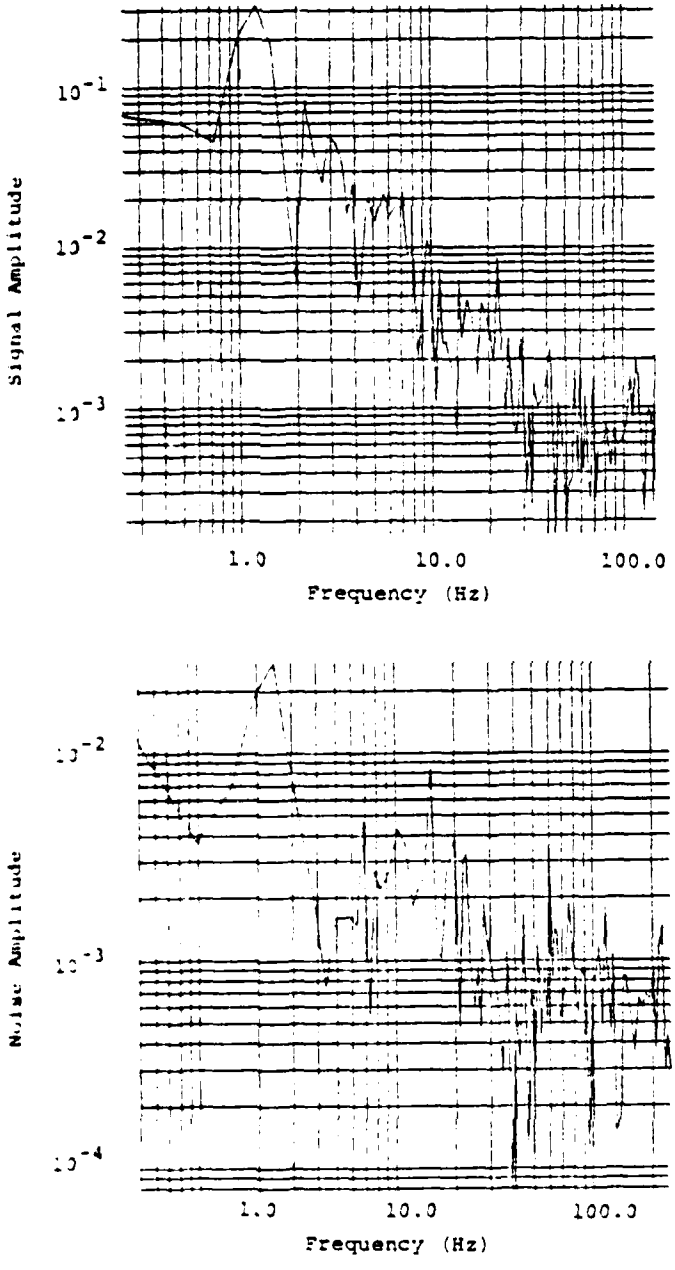

Figure 3.14. Fourier amplitude spectra for the original signal and noise sample at Station 7 of the MAST explosion.

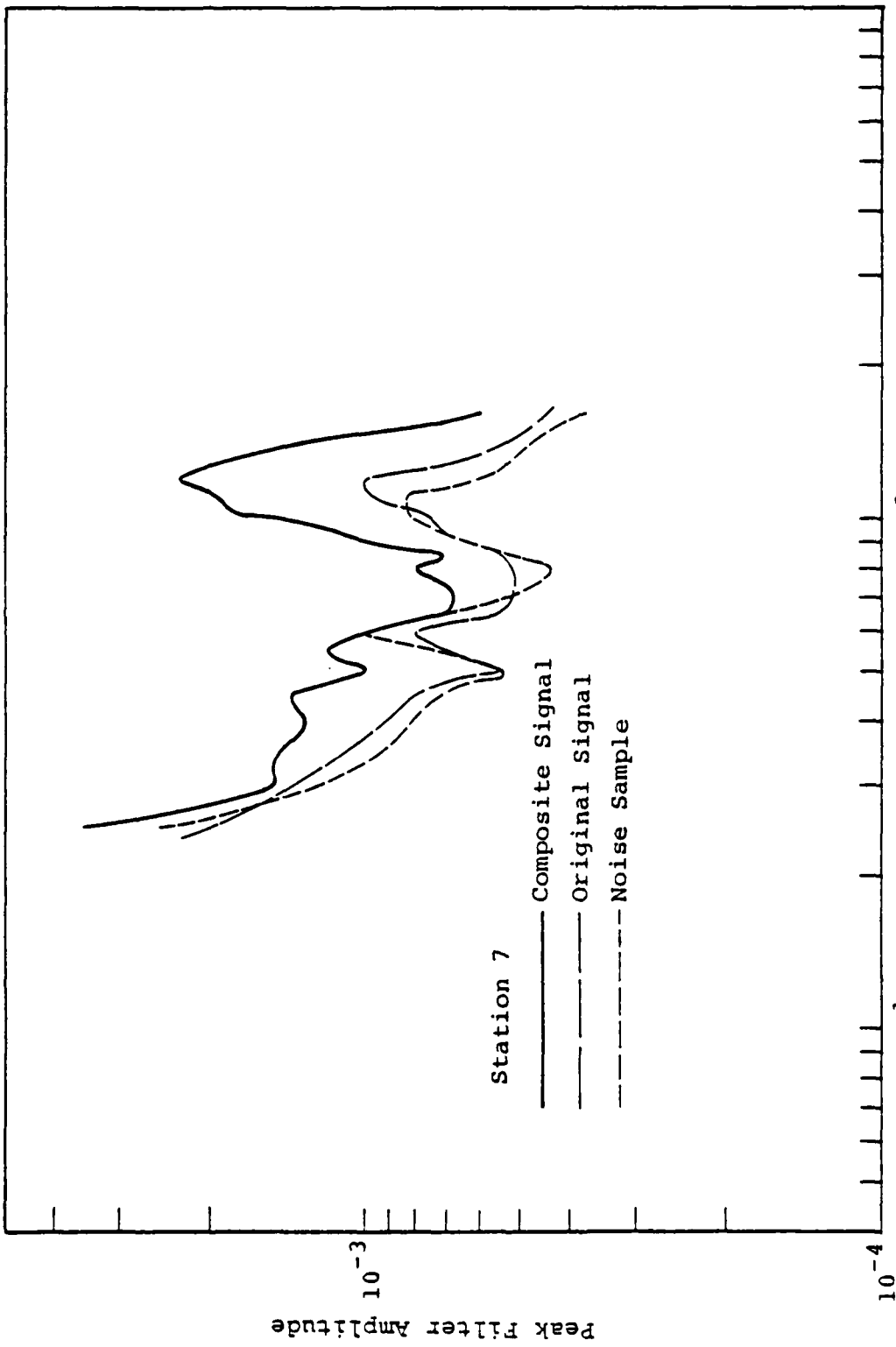

Figure 3.15. Narrow band peak filter amplitudes for the composite signal and original signal-noise sample at Station 7.

summation may have increased the degree of difficulty for separating out the desired events.

3.2.6 Summary and Discussion

Close-in seismic data obtained from Sandia for the underground nuclear explosion MAST have been used to simulate a simple multiple explosion. This multiple explosion consisted of three equal sized (150 kt) aligned explosions (separated by 355 m) detonated at the same instant. Two profiles were simulated, one in-line with the explosion array and the other oriented at 45° to the explosion array. Seismic records for the multiple event were synthesized by simple summation of one MAST seismic record to the same record with appropriate delay times. The determination of the delay times was based on the orientation of the two hypothetical station arrays relative to the explosion array, actual station distances from MAST and a compressional velocity of 3.8 km/sec.

Application of a series of cusp-shaped narrow band filters, with center frequencies (f_c) ranging from 25 Hz to 160 Hz, to the synthesized multiple explosion records yielded the following results:

- Accurate relative amplitude and time separation between explosions was achieved at the very close stations and, in particular at distances of less than 1.5 kilometers. Beyond 1.5 kilometers the signal-to-noise ratio is too low in the high frequency band of analysis to obtain definitive results.
- Separation between explosions was observed to begin at frequencies 3.5 times the explosion frequency (inverse of the explosion delay times). In general, separation of events becomes more distinct with increasing frequency.

In conclusion, when there is sufficient high frequency signal energy present, narrow band filtering is able to accurately scale the relative amplitudes and time differences between individual explosions, at least for this simple multiple explosion simulation. We have not discussed absolute scaling of amplitudes to determine actual yields. However, if we know either the yield of an individual explosion or the yield of the total array, we can scale the individual events from the relative amplitudes separated out by the narrow band filters.

3.3 THREE-DIMENSIONAL SEISMIC MODELING EXPERIMENT

Preparations are nearing completion for the first of four main experiments with three-dimensional seismic models. Figure 3.16 shows the four planned experimental configurations. In Figure 3.16a we have a deeply buried single source shot with measurements on the free surface. In Figure 3.16b the source is near the surface and will crater. The other two experiments are like those in Figure 3.16a and b except that three closely spaced sources will be used in each case with simultaneous detonation. Except for the change in position and number of sources, these experiments should be as identical as possible. The experimental results will be compared with calculations of the four models. The major tasks to be performed prior to the experiments are selections of material, source, detectors, and experimental geometry.

3.3.1 Material

We have selected a grout material that is similar to concrete except that it contains fine sand and no larger aggregate. We have tested three grouts and have chosen the one given in Table 3.2 because of its desirable properties and the ease of preparation in bulk. The other two grouts tested had satisfactory properties, but one had a larger grain size and the other required special materials, such as barite, that were not convenient to use in commercial handling. For the main experiment we plan to cast four blocks from the same mix.

3.3.2 Explosive Source

For a source we have purchased special spherical charges from Stanford Research Institute. These were recently developed by D. C. Erlich [1975], who had the goal of

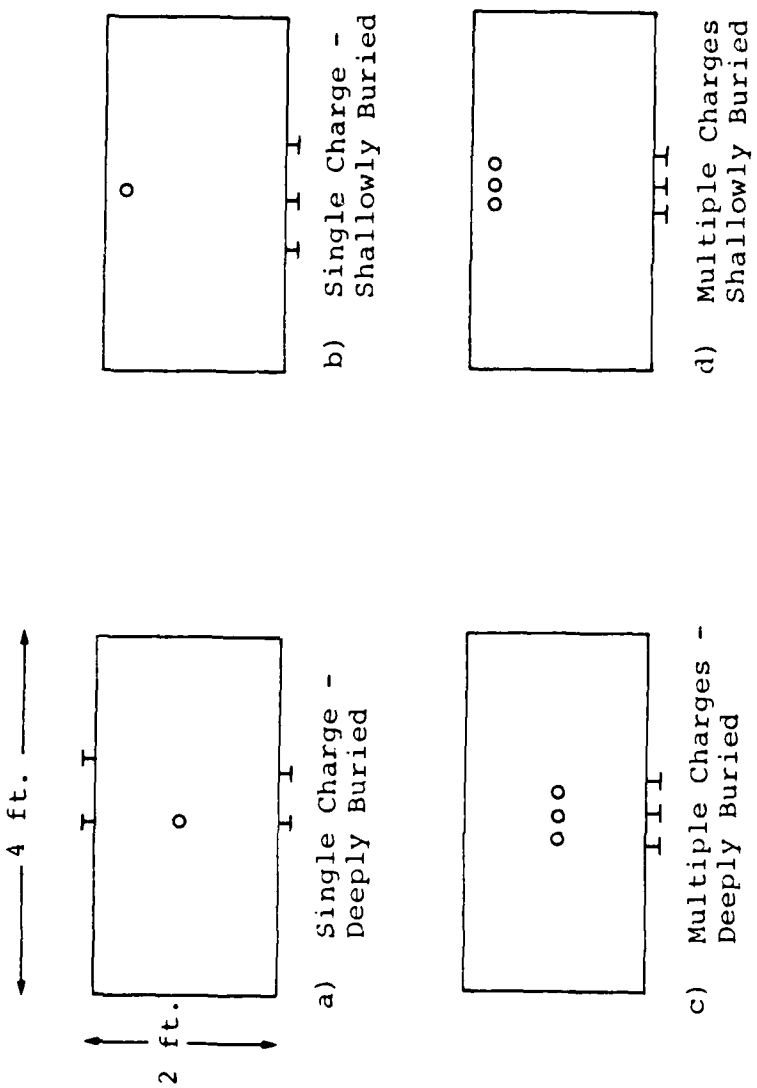

Figure 3.16. Four experiment types planned.

TABLE 3.2
GROUT COMPOSITION
(PER CUBIC YARD OF GROUT)

CEMENT	1128 lb
SAND (60-80 mesh)	2268 lb
POZZOLAN (300 R)	33.8 oz
AIR DE-ENTRAINING AGENT	12 oz
WATER	56 gal

Nominal properties: Unconfined compressive strength, 4400 psi (30 MPa)
Bulk density, 2.1 g/cm^3
Compressional velocity, 4.0 km/sec

developing a very small spherical explosive source for use in three-dimensional seismic modeling experiments. The explosive is 5/16-inch in diameter and is encased in a lucite shell of 1/16-inch wall thickness. The PETN is soft-pressed to a density of 1.0 g/cm^3, making a total of 0.26 g of PETN for the charge. The exploding bridgewire (EBW) in the center of the sphere is a 0.003-inch-diameter manganin wire soldered across a 0.010-inch gap between two 0.001-inch-thick copper leads emerging from one side of the lucite shell through a gap in the shoulder. Before casting the charge into the grout block, we will thoroughly waterproof the sphere and leads. The EBW is initiated with a standard detonating unit, which contains a fast trigger to dump the energy stored in a large capacitor.

3.3.3 Detectors

One major problem has been in obtaining useful detectors. We want to record the wave motion in both vertical and horizontal components. (Horizontal means parallel to the surface in the direction between the detector and the source.) In two-dimensional experiments (Cherry et al, 1975) PZT bender bimorph transducers were successfully used and found to respond at frequencies as high as 500 kHz. Robinson (1967) describes an arrangement of two bender bimorphs that he used to record two components of motion in three-dimensional experiments. Robinson found the detector useful for the 20 to 700 kHz range. We first tried an arrangement similar to Robinson's, but we found positioning and calibration to be very difficult. The detector was more suited to experiments where the source is repeated many times, and alignment and matching can be adjusted and checked until they are right. We also did not find a good calibration procedure.

After briefly trying some other detectors, including stereophonograph pickups, we built the detector shown in

Figure 3.17. The two bimorphs (Gulton G-1195) are mechanically connected and electronically isolated. Vertical motion causes the upper member to bend in the center, generating a signal. A horizontal motion bends the lower member, which is glued to the surface, generating a signal on that crystal.

We are still in the process of checking and calibrating this detector. Resonances occur at a few thousand hertz, depending on the size and configuration of the detector and its holder. We are interested in higher frequencies (probably 10 to 50 kHz) and have not seen any resonances above 10 kHz. The two main problems remaining are calibration and establishing that the two detectors record motions independently of each other.

For calibration we have set up our VISAR (Velocity Interferometer System for Any Reflector) to examine motions of the surface near the gauge or to examine motions of the gauge itself. For this application the VISAR is operating in the displacement mode, essentially as a Michelson interferometer. A laser is used to supply enough light that we can look directly at a diffuse reflecting surface. As a result of this work we have verified that the detector is tracking properly in the vertical mode and that resonance is not a difficult problem. We have identified some problems in mounting the gauge that have required some modifications. Figure 3.18 shows a tracing of an oscilloscope recording of the detector response. The source of motion was a pulse delivered to a small loudspeaker. The lower record is the vertical component of the detector, and the middle record is the output from the interferometer. The upper record is the reduction of the interferometer output to a displacement record. The agreement is fairly good, except that the large oscillations of the loudspeaker are seen to attenuate in the interferometer record and do not in the bimorph detector record. We determined that this was caused by motion of the detector holder, which depended only on its inertia to hold its position in

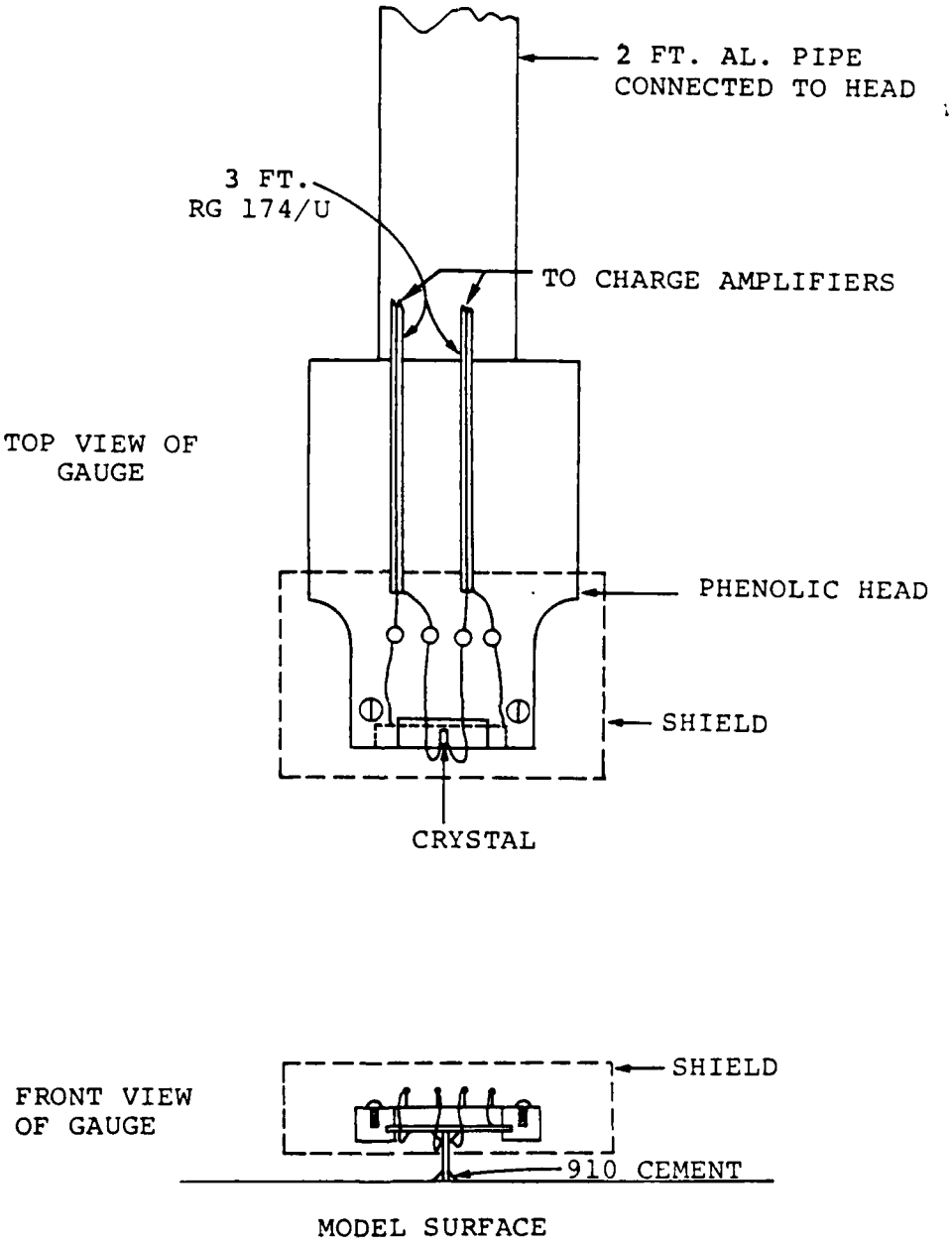

Figure 3.17. Bidirectional detector for grout model experiments.

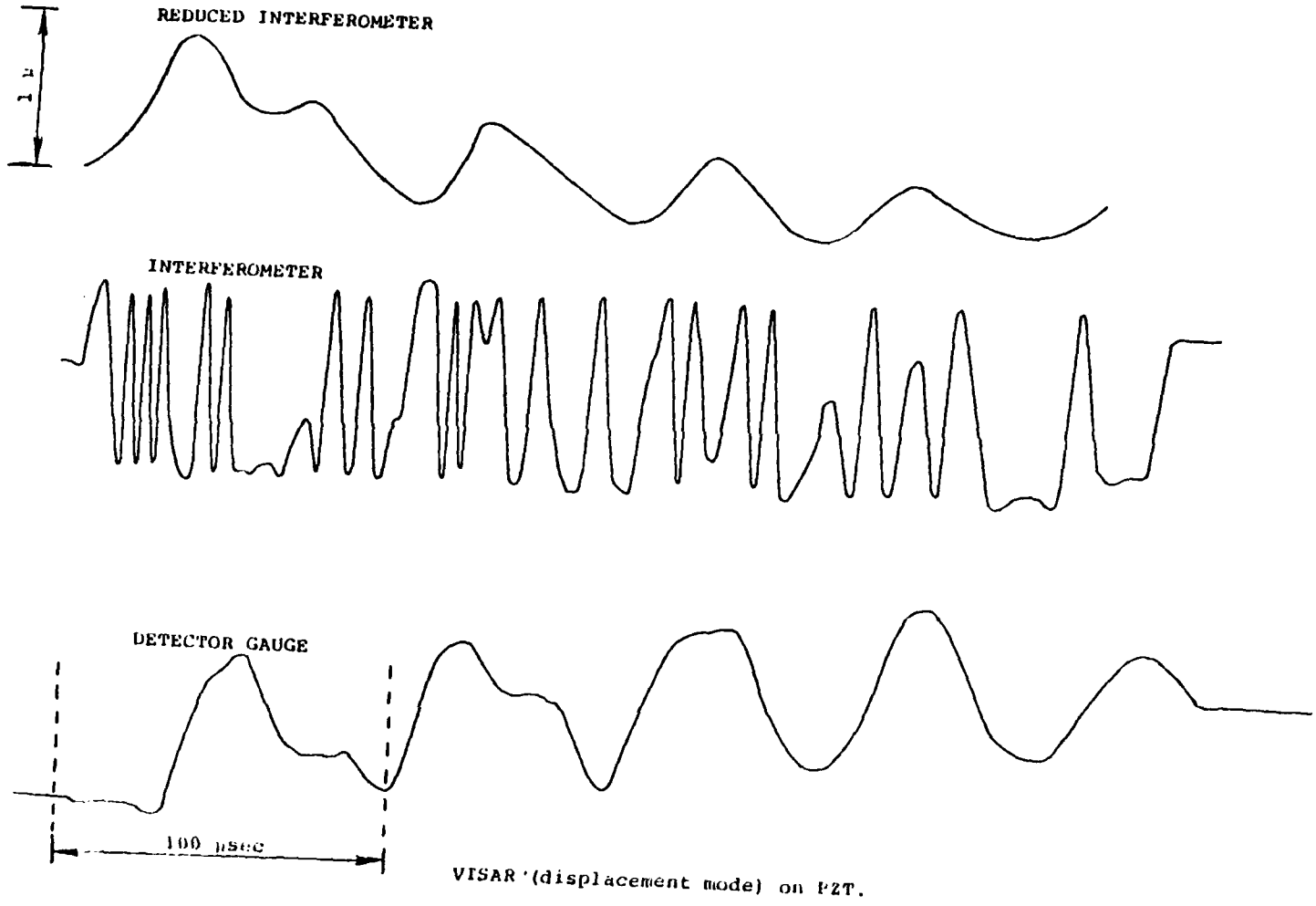

Figure 3.18. Tracing of records from detector (lower), interferometer (middle), and reduced interferometer record (upper).

these tests. The detector holder will be more firmly fixed in position for the block experiments. In our actual experiments, the recording time of interest will be about 100 μs.

We have also checked the horizontal component for calibration and for independence of output from the vertical component. About 10% of the vertical output was picked up on the horizontal component.

3.3.4 Experiments

Two grout blocks, each 4 ft. in diameter and 2 ft. thick, have been poured at our test site. These are being kept covered and wet. As soon as we are satisfied that the detectors are operating properly, we will proceed with the first experiment. For this one we will grout the explosive (with the same grout) near the center of the block, nominally nine inches from one flat surface and 15 inches from the other. Detectors will be mounted on both sides to record at two ranges. After firing the first shot we will core the center of the block to examine the cavity formed and to check for any asymmetrical aspects of the shot. We will also take cores for measurement of material properties. The second experiment will probably duplicate the first, unless results of the first suggest modifications.

IV. REFERENCES

Bache, T. C., J. T. Cherry, K. G. Hamilton, J. F. Masso and J. M. Savino [1975], "Application of Advanced Methods for Identification and Detection of Nuclear Explosions from the Asian Continent," Systems, Science and Software Semi-Annual Report, SSS-R-75-2646.

Bache, T. C., T. G. Barker, J. T. Cherry and J. M. Savino [1976], "Teleseismic Verification of Data Exchange Yields," Systems, Science and Software Topical Report, SSS-R-76-2941 (Draft).

Cherry, J. T., T. C. Bache and D. F. Patch [1975], "The Teleseismic Ground Motion Generated by a Nuclear Explosion Detonated in a Tunnel and its Effect on the M_S/m_b Discriminant," Systems, Science and Software Final Report, DNA 3645F.

Cooley, J. W. and J. W. Tukey [1965], "An Algorithm for the Machine Calculation of Complex Fourier Series," Mathematics of Computation, 19, pp. 297-301.

Erlich, D. C. [1975], "Three-Dimensional Seismic Modeling," Stanford Research Institute Final Report to Air Force Cambridge Research Laboratories, AFCRL-TR-75-0478.

Helmberger, D. V. and R. A. Wiggins [1971], "Upper Mantle Structure of the Midwestern United States," Journal of Geophysical Research, 76, pp. 3229-3245.

Robinson, D. J. [1967], "Bidirectional Detector of Ultrasonic Particle Motion in Solids," Review of Scientific Instruments, 38, pp. 813-814.

Savino, J. M., T. C. Bache, J. T. Cherry, K. G. Hamilton, D. G. Lambert and J. F. Masso [1975], "Application of Advanced Methods for Identification and Detection of Nuclear Explosions from the Asian Continent," Systems, Science and Software Semi-Annual Technical Report, SSS-R-76-2792.

Wiggins, R. A. and D. V. Helmberger [1973], "Synthetic Seismogram Computation for Expansion in Generalized Rays," Geophys. J. R. Astr. Soc., 37, pp. 73-90.

APPENDIX A

NARROW BAND FILTER OUTPUTS FOR STATIONS S-2 THROUGH S-7 ALONG THE PROFILE ORIENTED 45° TO THE EXPLOSION ARRAY

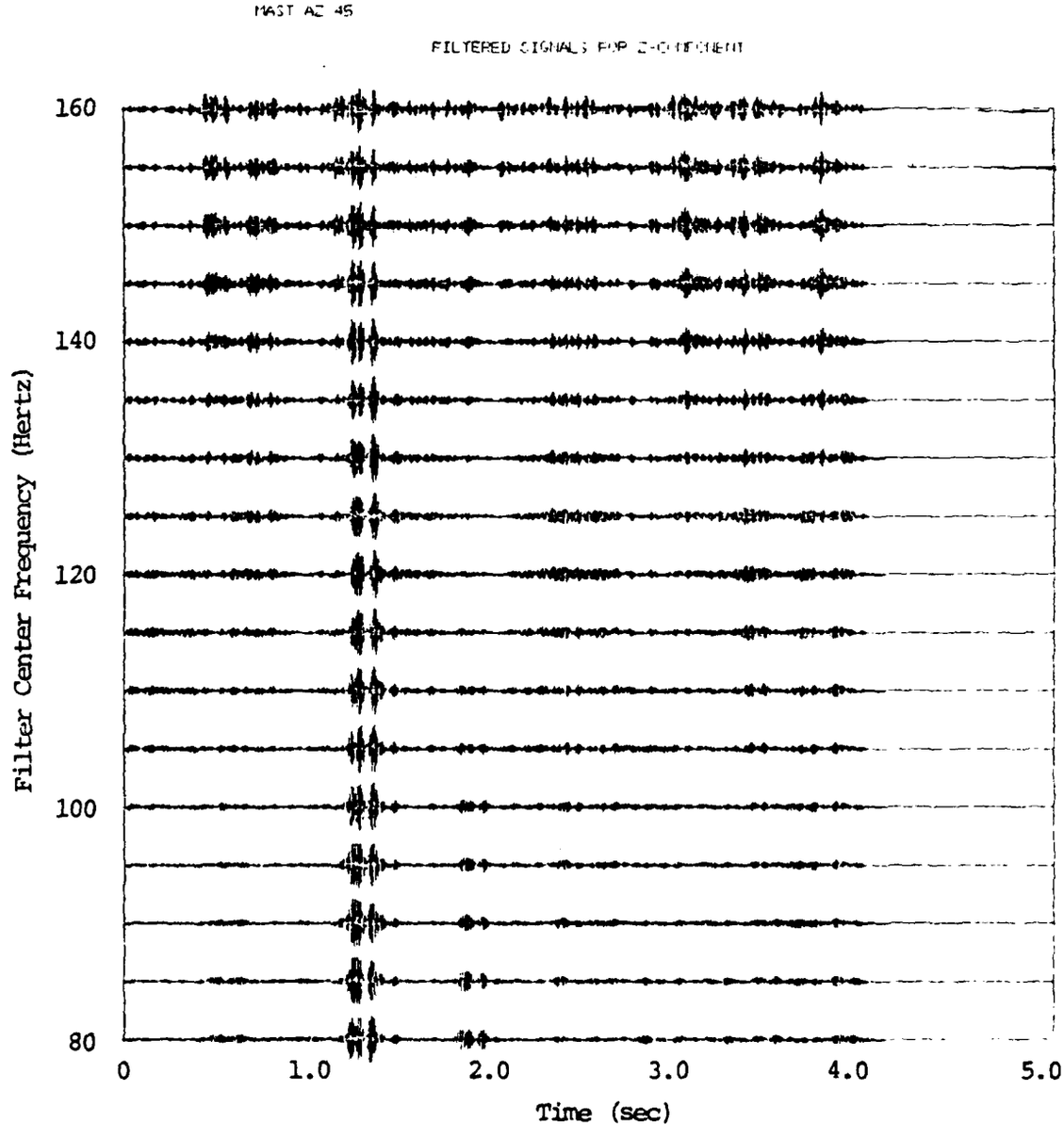
MAST AZ 45
FILTERED SIGNALS FOR Z-COMPONENT
160
140
120
100
80
Filter Center Frequency (Hertz)
0
1.0
2.0
3.0
4.0
5.0
Time (sec)

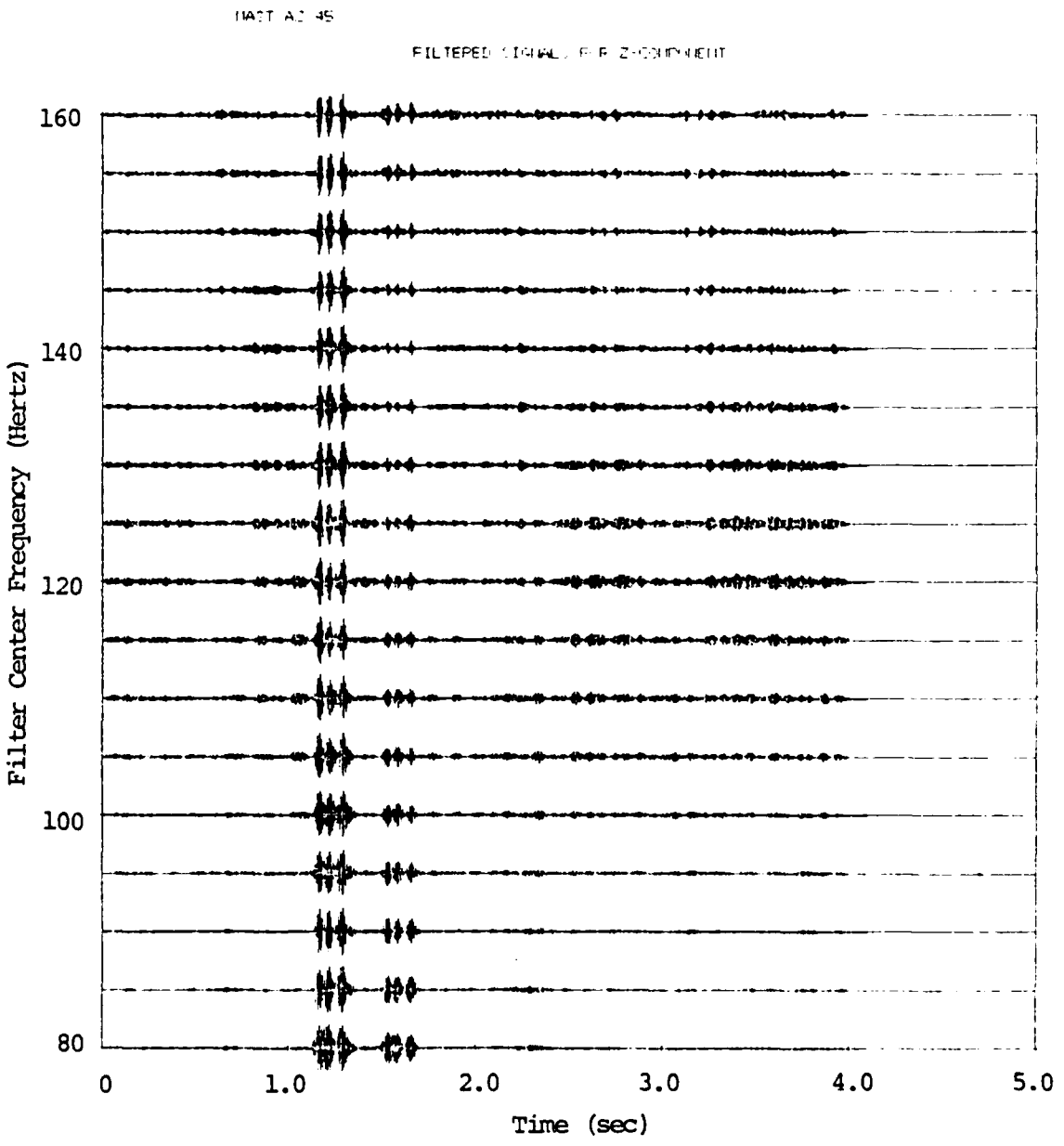
160
140
120
100
80
Filter Center Frequency (Hertz)
0
1.0
2.0
3.0
4.0
5.0
Time (sec)

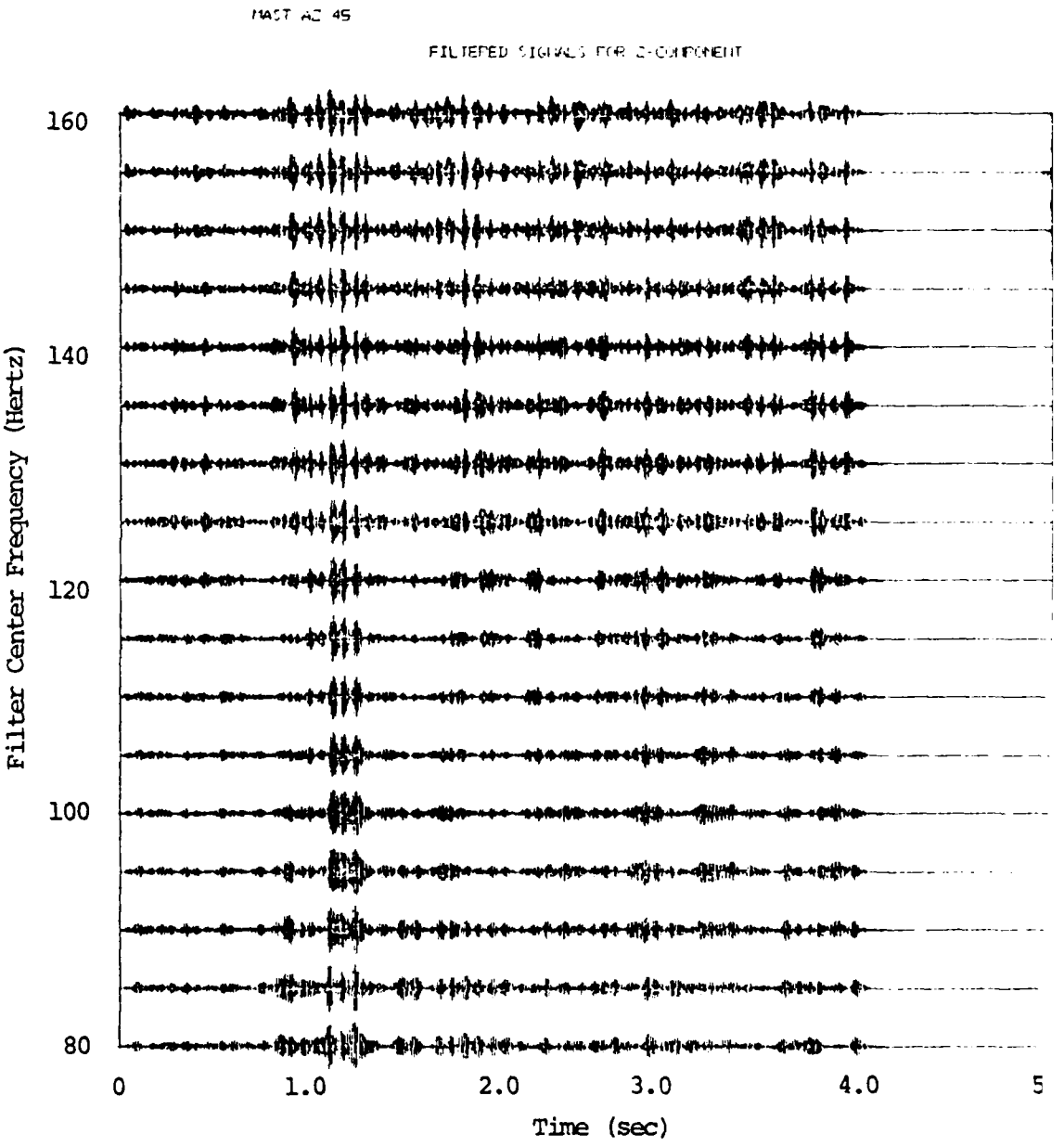
MAST AZ 45
FILTERED SIGNALS FOR Z-COMPONENT
160
140
120
100
80
Filter Center Frequency (Hertz)
0
1.0
2.0
3.0
4.0
5
Time (sec)

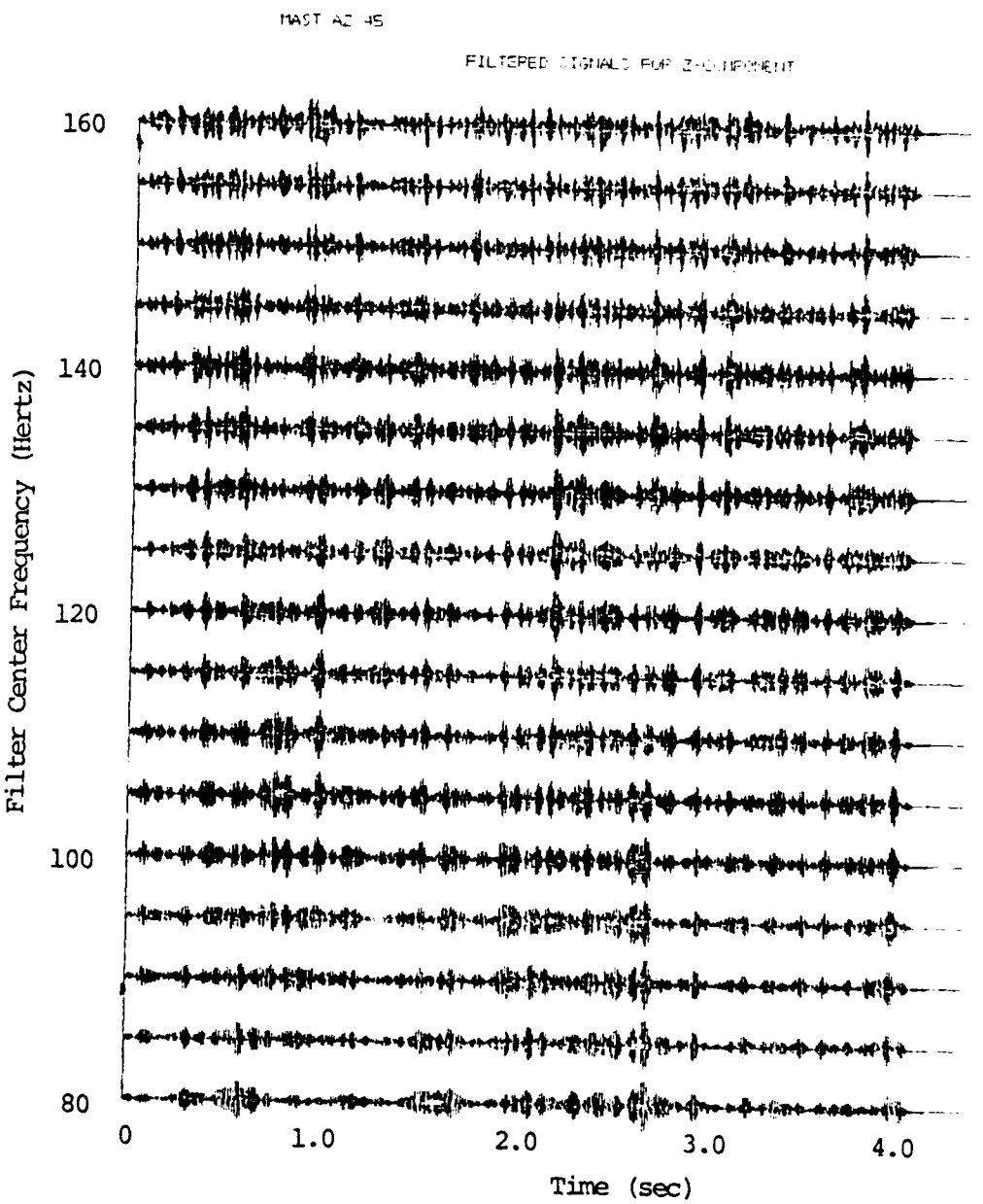
MAST AZ 45
FILTERED SIGNALS FOR Z-COMPONENT
160
140
120
100
80
Filter Center Frequency (Hertz)
0
1.0
2.0
3.0
4.0
Time (sec)

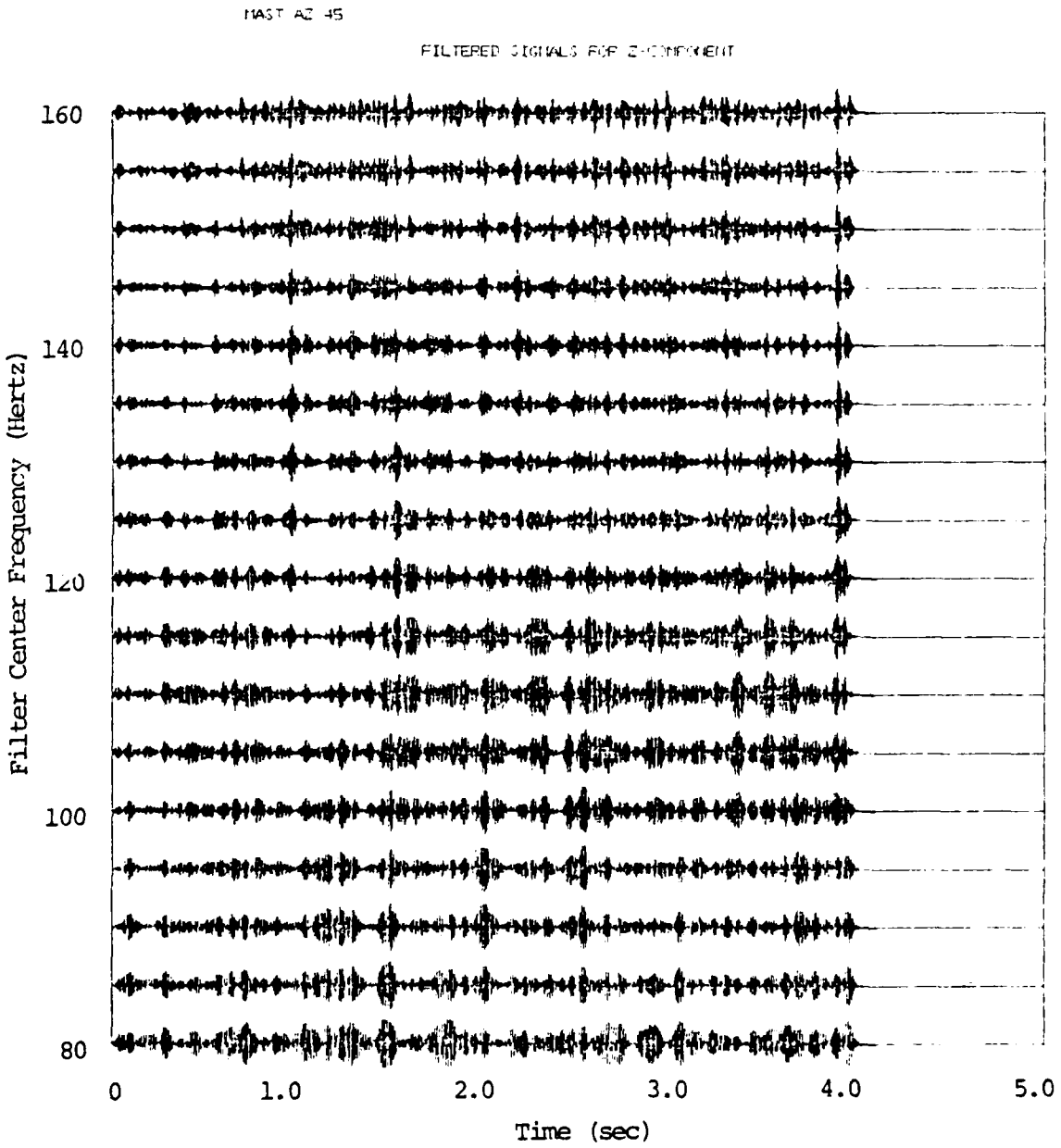
MAST AZ 45
FILTERED SIGNALS FOR Z-COMPONENT
160
140
120
100
80
Filter Center Frequency (Hertz)
0
1.0
2.0
3.0
4.0
5.0
Time (sec)

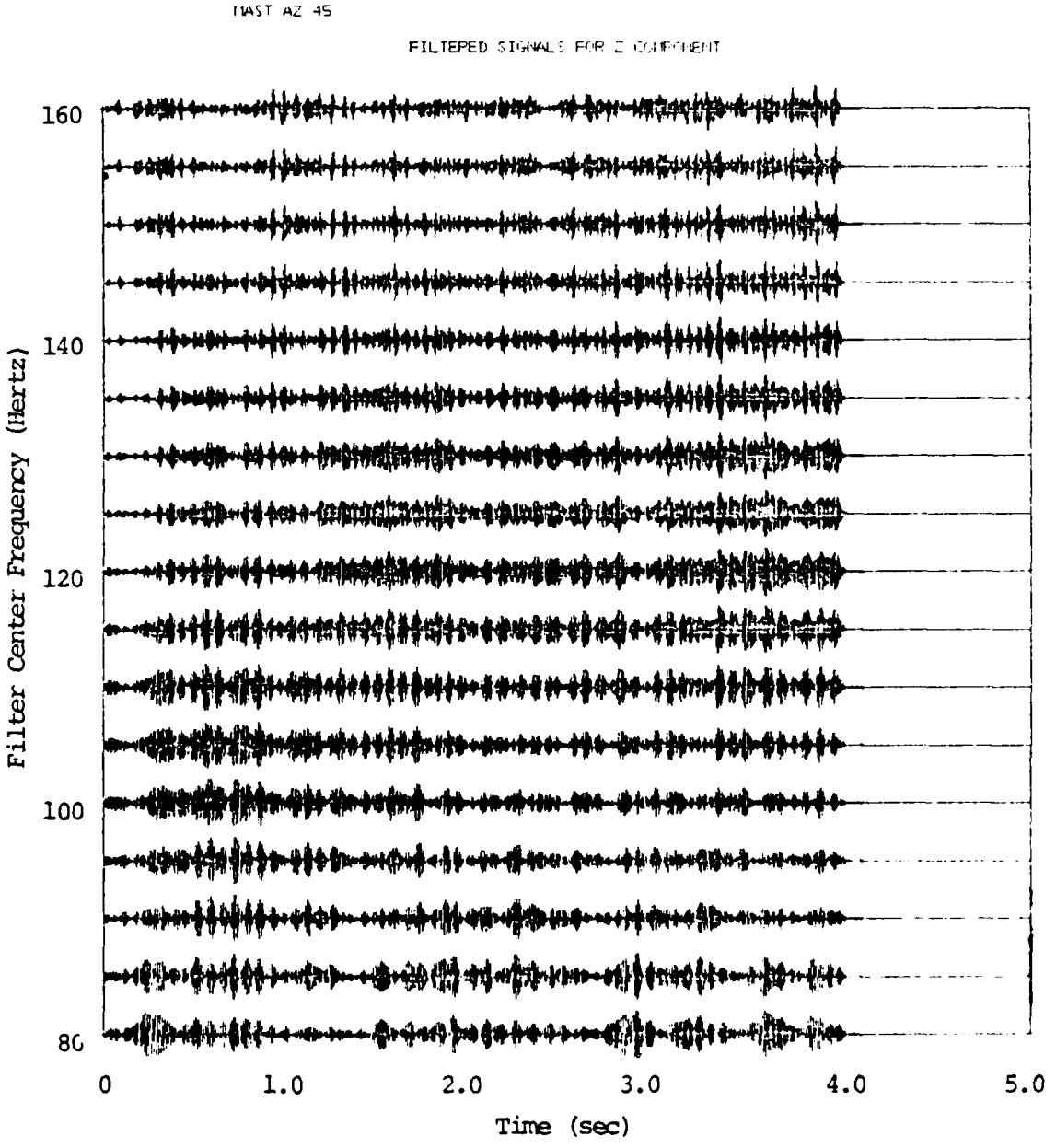
MAST AZ 45
FILTERED SIGNALS FOR Z COMPONENT
160
140
120
100
80
Filter Center Frequency (Hertz)
0
1.0
2.0
3.0
4.0
5.0
Time (sec)